

# Exact nonequilibrium dynamics of a class of initial states in one-dimensional two-component integrable quantum gases

Neil J. Robinson,<sup>1,\*</sup> Jean-Sébastien Caux,<sup>2,†</sup> and Robert M. Konik<sup>1,‡</sup>

<sup>1</sup>*Condensed Matter Physics and Materials Science Department,  
Brookhaven National Laboratory, Upton, NY 11973-5000, USA*

<sup>2</sup>*Institute for Theoretical Physics, University of Amsterdam,  
Science Park 904, 1098 XH Amsterdam, The Netherlands*

(Dated: December 3, 2024)

We present the numerically exact time-evolution of a class of initial states in integrable one-dimensional two-component quantum gases. This special class of states, formed from a simple superposition of eigenstates, contains a well-localized particle of one species and a background gas containing a density-depletion (hole) in the vicinity of this particle, looking much like an exciton. The special structure of the initial states means that we can compute the time-evolution in a numerically exact manner for large numbers  $N = 100 - 1000$  of interacting particles, comparable with those studied in experiments on cold atomic gases. The initial state can be pictured as a linear superposition of spin wave excitations, and has significant overlap with simple spin flip excitations, which have been studied in existing experimental setups. We study both fermionic and bosonic quantum gases and highlight some differences between the two cases. In both cases, the initially well-localized exciton dissolves, with particle-hole excitations spreading through the gas within a light cone. The behavior of the light cone on varying the interaction strength and density of the gas can be understood from existing exact results for the spin wave mass in these systems. Within the light cone of the Bose gas, we see evidence of additional excitations about (finite momentum) roton-like minima in the spin wave dispersion.

PACS numbers: 02.30.Ik,03.75.-b,67.85.-d,67.85.De,67.85.Fg

## I. INTRODUCTION

Predicting and understanding the nonequilibrium dynamics of strongly correlated quantum systems presents a huge challenge in contemporary physics [1–3]. The study of integrable quantum systems has been key in significantly advancing our understanding of such problems. This special class of systems can be exactly solved using well-known techniques [4, 5] and, in some cases, their nonequilibrium dynamics computed analytically, see for example Refs. [6–14]. These studies have highlighted the important role of local (and quasi-local) conservation laws in constraining the nonequilibrium dynamics and relaxation of isolated systems; the presence of additional constants of motion prevents thermalization [6–37]. Instead, expectation values of local operators in subsystems relax to time-independent values described by a generalized Gibbs ensemble [6–37]. Importantly, such behavior and constrained dynamics can persist for intermediate time scales even when integrability is broken [38–50].

So far, most of the studies of the nonequilibrium dynamics of integrable models have been restricted to those models which contain a single species of particle, e.g. spin-1/2 chains or spinless fermions. This is due to a technical difficulty: there is a lack of knowledge of matrix elements of local operators in interacting multicom-

ponent systems. Perhaps the simplest example of such a system is the Yang-Gaudin model [51, 52] for a two-component quantum gas, described by the Hamiltonian

$$\mathcal{H} = \frac{\hbar^2}{2m} \sum_{\sigma=\uparrow,\downarrow} \partial_x \Psi_\sigma^\dagger(x) \partial_x \Psi_\sigma(x) + c \sum_{\sigma,\sigma'=\uparrow,\downarrow} \Psi_\sigma^\dagger(x) \Psi_{\sigma'}^\dagger(x) \Psi_{\sigma'}(x) \Psi_\sigma(x), \quad (1)$$

where  $m$  is the mass of the (bosonic or fermionic) particles,  $\sigma = \uparrow, \downarrow$  is a (pseudo) spin index that labels the two particle species, and  $c$  is the interaction parameter. In this model, there has been significant progress over the last few years in obtaining efficient representations of matrix elements; the ‘extreme imbalance’ limit (a single particle of one of the species) was considered in Ref. [53], whilst recent advances in the study of form factors of  $GL(3)$ -invariant models [54–58] have opened the door to obtaining matrix elements of local operators in more general cases [58].

Understanding the dynamics and properties of such two-component quantum gases is important; they are ubiquitous and play a central role in condensed matter physics, as well as being routinely studied in experiments on cold atomic gases [59–62]. Recent advances in the latter field have given rise to unprecedented levels of control and tuneability of the system, both in terms of isolation of the system from the environment and in the systematic control of the strength and form of interactions and kinetics. Precise control over the constituents of the gas has enabled the study of the ‘extreme imbalance’ limit [63–

\* nrobinson@bnl.gov

† J.S.Caux@uva.nl

‡ rmk@bnl.gov

70], which one can picture as a single distinguishable impurity immersed in a bath. The nonequilibrium dynamics of such an impurity have been the subject of extensive experimental [63–70] and theoretical [71–87] investigation.

In this work, we focus on the extreme imbalance limit of the Yang-Gaudin model of two-component quantum gases (1) and consider the nonequilibrium dynamics of a special class of initial states. These states, constructed from a simple linear superposition of eigenstates, contains a single well-localized exciton-like density configuration and have significant overlap with ‘spin flip’ excitations studied in experiments on cold atomic gases [65]. Due to the simple structure of this class of states, we can compute the *numerically exact* time-evolution for very large numbers ( $N = 100 - 1000$ ) of interacting particles, comparable to system sizes studied in existing experiments on one-dimensional cold atomic gas (see, e.g., Ref. [68]).

We proceed as follows: in Sec. II A we will first detail the solution of Yang-Gaudin Fermi gas via the Bethe ansatz and discuss some of its known properties. Section II B will take a brief aside to introduce how we compute observables via the matrix element expansion. Following this, in Sec. II C we introduce the special class of initial states that we consider, and we discuss their relation to simple ‘spin flip’ states which have been studied in experiments [65]. Having introduced the state, we then discuss its nonequilibrium dynamics in Sec. II D. In Sec. III we then give a similar sequence of discussion for the Yang-Gaudin Bose gas, highlighting some important differences to the fermionic case. We conclude in Sec. IV and present some additional and complementary data in the Appendix.

## II. FERMIONS

### A. The Yang-Gaudin Fermi gas

The Yang-Gaudin Hamiltonian (1) describes a system of two-component particles interacting via a delta-function potential with strength  $c$ . In this work, we focus on the case where the interaction is repulsive  $c > 0$  and we impose periodic boundary conditions; a system of  $N$  particles is placed on a ring of circumference  $L$ . Herein, we work in units where  $\hbar = 2m = 1$  and it will be useful to consider the dimensionless interaction parameter  $\gamma = 2mc/\hbar^2 \varrho$ , where  $\varrho = N/L$  is the average particle density.

#### 1. Solution via the Bethe ansatz

Let us begin by considering the Yang-Gaudin model (1) with spin-1/2 fermion fields

$$\left\{ \Psi_\sigma(x), \Psi_{\sigma'}^\dagger(y) \right\} = \delta_{\sigma\sigma'} \delta(x-y), \quad (2)$$

where  $\sigma = \uparrow, \downarrow$  labels the spin-1/2 degree of freedom. The fermionic Yang-Gaudin model (1) is integrable and exactly solvable via the (nested) Bethe ansatz [5, 51, 52, 88]. An eigenstate containing  $N$  particles, of which  $M$  have flipped spins, is characterized by two sets of quantum numbers: a set of  $N$  quasi-momenta  $\{p\} \equiv \{p_1, \dots, p_N\}$  and  $M$  spin rapidities  $\{\lambda\} \equiv \{\lambda_1, \dots, \lambda_M\}$ . These quantum numbers satisfy the logarithmic Bethe ansatz equations

$$\begin{aligned} 2\pi \tilde{I}_j &= p_j L + \sum_{\alpha=1}^M \phi_2(p_j - \lambda_\alpha), \\ 2\pi \tilde{J}_\alpha &= \sum_{j=1}^N \phi_2(\lambda_\alpha - p_j) - \sum_{\beta=1}^M \phi_1(\lambda_\alpha - \lambda_\beta), \end{aligned} \quad (3)$$

where the scattering phase  $\phi_n(u)$  is given by

$$\begin{aligned} \phi_n(u) &= i \log \left( \frac{\frac{ic}{n} + u}{\frac{ic}{n} - u} \right), \\ &\equiv 2 \arctan \left( \frac{un}{c} \right), \end{aligned} \quad (4)$$

and we have defined the ‘integers’  $\tilde{I}_j, \tilde{J}_\alpha$  which satisfy

$$\tilde{I}_j \in \begin{cases} \mathbb{Z}, & \text{if } M \in 2\mathbb{Z}, \\ \mathbb{Z} + \frac{1}{2}, & \text{if } M \in 2\mathbb{Z} + 1, \end{cases} \quad (5)$$

$$\tilde{J}_\alpha \in \begin{cases} \mathbb{Z}, & \text{if } (N+M) \in 2\mathbb{Z} + 1, \\ \mathbb{Z} + \frac{1}{2}, & \text{if } (N+M) \in 2\mathbb{Z}, \end{cases} \quad (6)$$

The integers obey an exclusion principle:  $\tilde{I}_i \neq \tilde{I}_j$  if  $i \neq j$ ,  $\tilde{J}_\alpha \neq \tilde{J}_\beta$  if  $\alpha \neq \beta$ . The ground state is formed from the ‘Fermi sea’ of integers  $\tilde{I}_j$ , a symmetric distribution of the integers about 0. The eigenstate  $|\{p\}; \{\lambda\}\rangle$  has momentum  $P_{\{p\}}$  and energy  $E_{\{p\}}$ , which are given solely in terms of the quasi-momenta

$$P_{\{p\}} = \sum_{j=1}^N p_j = \frac{2\pi}{L} \left( \sum_{j=1}^N \tilde{I}_j - \sum_{\alpha=1}^M \tilde{J}_\alpha \right), \quad (7)$$

$$E_{\{p\}} = \sum_{j=1}^N p_j^2. \quad (8)$$

The integrability of the model is realized in the constants of motion, which can also be constructed from the quasi-momenta  $\mathcal{I}_n = \sum_{j=1}^N p_j^n$ , with  $n \in \mathbb{N}$ .

#### 2. Known properties

The Yang-Gaudin Fermi gas, as one of the simplest examples of an interacting multicomponent quantum gas, has been extensively studied since its exact solution in 1967 [51, 52]. Its equilibrium properties are well understood [62]; the zero-temperature ground state was shown by Lieb and Mattis to be unpolarized [89], the ground state and low-energy excitations were extensively studied by Schlottmann [90, 91], and the finite-temperature

thermodynamics has recently been considered [92]. The strong coupling limit  $c \rightarrow \infty$  describes the low-density limit of the Hubbard model [93]. In states with non-zero polarization the phase diagram has been studied, both via the Bethe ansatz and in experiments on cold atomic gases [94]; the spin-imbalanced Yang-Gaudin Fermi gas is a prime candidate for the observation of Fulde-Ferrell-Larkin-Ovchinnikov superconductivity [95, 96]. The fully polarized state has been prepared experimentally and used to study deviations from the Yang-Gaudin Fermi gas due to  $p$ -wave scattering [97]. Experiments in cold atoms have also studied the formation of bound state [98] and the addition of an optical lattice (cosine potential) [99].

### 3. Excitations of Yang-Gaudin gases

The Yang-Gaudin model (1) has an  $SU(2)$  symmetry; the eigenstates can be classified according to their (pseudo) spin  $S$ , ranging from  $S = 0$  to  $S = N/2$ . The nature of the zero temperature ground state is surprisingly different for fermions and bosons; the fermionic ground state is not magnetized [89], whilst the bosonic ground state is completely polarized  $S = N/2$  [100, 101].

Two types of excitations arise with the Yang-Gaudin gas, which can be related to the integers appearing within the logarithmic Bethe ansatz equations (3). The first type of excitation, which we will call a ‘charge’ excitation, can be constructed by creating particle-hole excitations upon the Fermi sea of integers  $I_j$  (e.g., moving one or more of the integers beyond the largest value in the ground state configuration, leaving behind ‘holes’). Secondly, there are ‘spin’ excitations which correspond to the presence of integers  $J_\alpha$ . For  $M > 1$  the spin rapidities  $\lambda_\alpha$  organize in to strings in the complex plane, representing bound states.

For models possessing an  $SU(2)$  symmetry, general considerations [102, 103] impose that spin wave excitations above the fully polarized state have quadratic dispersion at small momentum  $p \ll \varrho$

$$E(p) - E(0) \approx \frac{p^2}{2m^*}, \quad (9)$$

where  $m^*$  is the effective mass for the spin wave excitation. At strong coupling this effective mass  $m^*$  can become very large  $m^* \propto N$  [104–106], and this is responsible for the unusual “logarithmic diffusion” observed in the low-energy behavior of dynamic correlation functions in the Yang-Gaudin Bose gas [106].

### B. Time-evolution via matrix element expansion

Let us now take a brief aside and discuss how we compute observables and their time-evolution. We consider an arbitrary state  $|\phi\rangle$ ; in the basis of eigenstates of the

Hamiltonian (1) it may be expressed as

$$|\phi\rangle = \sum_{\{p\},\{\lambda\}} c_{\{p\},\{\lambda\}}^\phi |\{p\};\{\lambda\}\rangle, \quad (10)$$

where  $c_{\{p\},\{\lambda\}}^\phi = \langle\{p\};\{\lambda\}|\phi\rangle$  are normalized such that  $\langle\phi|\phi\rangle = 1$ . Time-evolution of the state  $|\phi\rangle$  is straightforward: each eigenstate in the superposition picks up a phase factor under the time-evolution

$$e^{-iHt}|\{p\};\{\lambda\}\rangle = e^{-iE_{\{p\}}t}|\{p\};\{\lambda\}\rangle. \quad (11)$$

The prescription for computing time-dependent expectation values is now clear. Provided we know the matrix elements of an operator  $\hat{O}(0)$ , we can directly compute its time-evolved expectation value

$$\begin{aligned} \langle\phi|\hat{O}(x,t)|\phi\rangle &= \sum_{\{p\},\{\lambda\}} \sum_{\{k\},\{\mu\}} \left(c_{\{p\},\{\lambda\}}^\phi\right)^* c_{\{k\},\{\mu\}}^\phi \\ &\times e^{it(E_{\{p\}} - E_{\{k\}})} e^{ix(P_{\{k\}} - P_{\{p\}})} \\ &\times \langle\{p\};\{\lambda\}|\hat{O}(0)|\{k\};\{\mu\}\rangle. \end{aligned} \quad (12)$$

For an arbitrary state, the sums over the eigenstates are, in fact, infinite sums and it is necessary to truncate the expansion by keeping only the ‘most important’ eigenstates. However, in the next section we will see that for a judicious choice of initial state this is no longer a necessity and the time-evolution can be computed in a *numerically exact* manner. The matrix elements of local operators  $\hat{O}(0)$  which we require have been recently derived from the algebraic Bethe ansatz [53, 58]; we note that determinant representations of matrix elements are crucial for efficient numerical evaluation of the dynamics, both in and out of equilibrium. Direct computations from the coordinate Bethe ansatz (see, for example, Ref. [107] for the Lieb-Liniger model) scale as  $(N!)^2$  and, as such, are limited to very small numbers of particles  $N \leq 7$ .

### C. A class of exciton-like initial states

We now construct a special class of initial states which are peculiar to two-component integrable models, and contain a single well-localized mobile exciton-like density configuration. Focusing on the ‘extreme imbalance’ limit, which contains a single flipped spin  $M = 1$ , our construction is inspired by the dark soliton yrast states found in the Lieb-Liniger model by Kaminishi *et al.* [108], whose numerically exact time-evolution has been studied for large numbers of particles [109–112]. However, the class of states that we consider is particular to multi-component models: the state is formed from a *linear superposition of eigenstates* with a fixed set of momenta integers  $\{I\}$  and the single spin rapidity integer  $J$  varied between its bounds

$$|\{I\}\rangle = \frac{1}{\sqrt{\mathcal{N}}} \sum_{|J| < \frac{\mathcal{N}}{2}} |\{p\}_J; \lambda_J\rangle. \quad (13)$$

Here  $\mathcal{N}$  is a normalization constant, and we introduce the notation  $\{p\}_J$  and  $\lambda_J$ , which denote the set of momenta and the spin rapidity associated with solving the logarithmic Bethe ansatz equations (3) with the configuration of integers  $\{I\}$  and the spin rapidity integer  $J$ . We are not restricted in our choice of the integers  $\{I\}$ ; in this work we will consider three particular cases:

1. The ground state configuration of integers, the ‘Fermi sea’,

$$\{I\}_0 = \left\{ -\frac{N-1}{2}, -\frac{N-1}{2} + 1, \dots, \frac{N-1}{2} \right\}. \quad (14)$$

2. The ‘diluted Fermi sea’, where every other integer is filled (symmetrically about zero)

$$\{I\}_s = \left\{ -\frac{2N-1}{2}, -\frac{2N-1}{2} + 2, \dots \right\}. \quad (15)$$

3. The ‘shifted Fermi sea’, where we construct a ‘Fermi sea’ with, e.g., the negative integers:

$$\{I\}_s = \left\{ -\frac{2N-1}{2}, -\frac{2N-1}{2} + 1, \dots \right\}. \quad (16)$$

We will particularly focus on the first case, where the initial state (13) can be pictured as a linear superposition of states which contain a spin wave excitation [105]. The momentum of the spin wave in each state of the superposition is given by  $P_{\{p\}_J}$  defined in Eq. (7). As we have focused on the ‘extreme imbalance’ limit, in the Yang-Gaudin Fermi gas we expect the initial state (13) to be highly excited, as it is far from the unpolarized ground state. For the Yang-Gaudin Bose gas, we expect the opposite: the constructed state will be a low-energy excitation, being close to the polarized ground state.

In the following two sections, we focus on the ground state configuration of integers and present the density of the initial state  $|\{I\}_0\rangle$  (14) and its relation to a simple experimentally relevant ‘spin flip’ state. We will return to the other configurations of integers when computing the nonequilibrium dynamics.

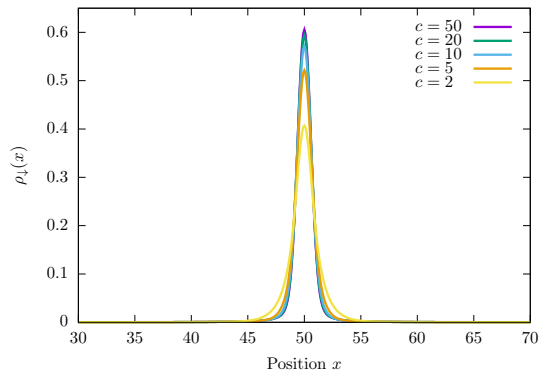
### 1. Density profile of the exciton-like state

Having introduced the initial state (13) in the previous section, let us begin by computing the initial density profile

$$\rho_\sigma(x) = \langle \{I\} | \Psi_\sigma^\dagger(x) \Psi_\sigma(x) | \{I\} \rangle, \quad (17)$$

composed with the ground state configuration of integers (14). In Fig. 1 we present the density for the two species  $\sigma = \uparrow, \downarrow$  of particles for a range of interaction strengths  $\gamma = c/\rho = 2 - 50$  for  $N = 100$  particles at unit density  $\rho = 1$ . The initial state with  $\{I\} = \{I\}_0$  contains a well-localized exciton-like density configuration, which becomes increasingly localized with strengthening interactions.

(a) Minority species  $\sigma = \downarrow$



(b) Majority species  $\sigma = \uparrow$

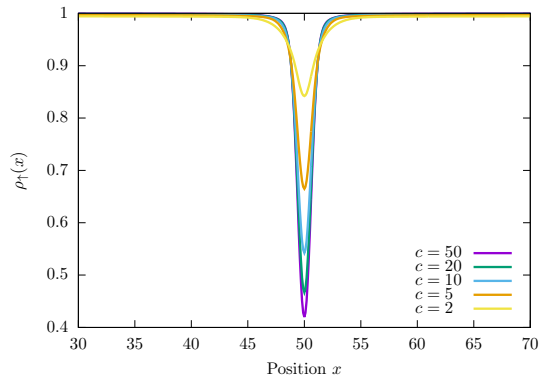


FIG. 1. **Fermions:** The density  $\rho_\sigma(x) = \langle \Psi_\sigma^\dagger(x) \Psi_\sigma(x) \rangle$  with (a)  $\sigma = \downarrow$ ; (b)  $\sigma = \uparrow$  for the exciton-like initial state (13) with the ground state configuration of integers (14). We consider  $N = 100$  particles at unit filling  $\rho = 1$  for a range of interaction strengths  $c = 2, 5, 10, 20, 50$ . Overlaps of the initial state with a simple spin-flip excitation (18) are shown in Table I.

### 2. Overlap with spin-flip excitation

Let us now address the following question: does the initial state (13) have a significant overlap with some simple-to-understand state, or are we constructing a state which is unlikely to be physically realized in experiment? In order to address this question, we consider a simple state which contains a spatially localized spin flip excitation

$$|sf\rangle = \frac{1}{\mathcal{N}} \int dx f(x) e^{iQx} \Psi_\downarrow^\dagger(x) \Psi_\uparrow(x) |\Omega\rangle, \quad (18)$$

where  $f(x)$  defines the shape of the spin flip excitation,  $|\Omega\rangle$  is an  $N$ -particle eigenstate of the one-component gas and  $Q$  is a center-of-mass momentum for the spin flip excitation. Each of these constituents can be chosen to maximize the overlap of the spin flip state  $|sf\rangle$  with the initial state (13); the scalar product  $\mathcal{C} = \langle \{I\}_0 | sf \rangle$  of the initial state with the spin flip excitation will give us a quantitative feel for how ‘close’ the two states are. We can compute the scalar product  $\mathcal{C}$  with knowledge of the matrix elements of the spin flip operator  $\Psi_\downarrow^\dagger(x) \Psi_\uparrow(x)$ ,

$\gamma$	$QL/2\pi$	Overlap $ \mathcal{C} $
2	3	0.3231
5	5	0.4260
10	6	0.4788
20	6	0.5052
50	6	0.5175
100	7	0.5208
500	7	0.5233

TABLE I. **Fermions:** Overlap of the initial state (13) with the localized spin flip excitation (18) in the Yang-Gaudin Fermi gas with momentum  $Q$ , chosen to maximize the overlap. We choose  $|\Omega\rangle$  to be the free fermion state with the Fermi sea of integers. The shape of the spin flip excitation,  $f(x)$  in Eq. (18), is chosen to reproduce the density of the impurity, see Fig. 1. Here we have used  $N = L = 30$ .

provided in Ref. [53]. We fix  $f(x)$  in (18) to reproduce the density of the  $\sigma = \downarrow$  component (see Fig. 1) and choose  $|\Omega\rangle$  to be the ground state of the one-component gas. Table I presents the overlap of the initial state with the spin flip excitation for a number of different interaction strengths with  $Q$  chosen to maximize the overlap. In all cases, we see that the initial state (13) has significant overlap with the spin flip excitation (18), especially at large values of the interaction strength. Importantly, states similar to  $|sf\rangle$  can be prepared experimentally [65], so we expect that our initial state (13) should capture at least some of the features of the nonequilibrium dynamics observed in experiments.

#### D. Non-equilibrium dynamics of the exciton-like state

We now consider the time-evolution of the initial state (13) in the Yang-Gaudin Fermi gas. As (13) is *not* an eigenstate of the Hamiltonian (1), we expect local observables to evolve in time. The central object of our study will remain the expectation value of the density operators

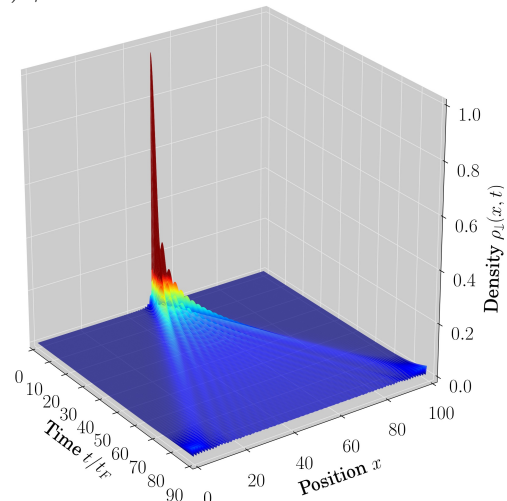
$$\rho_\sigma(x, t) = \langle \{I\} | e^{iHt} \Psi_\sigma^\dagger(x) \Psi_\sigma(x) e^{-iHt} | \{I\} \rangle, \quad (19)$$

which we compute by the matrix element expansion discussion in Sec. II B. In the following two sections, we will consider the weak coupling and strong coupling limits, respectively, of the time-evolution of the initial state (13) with the ground state configuration of the integers  $\{I\} = \{I\}_0$ . Following this, we examine the nonequilibrium dynamics with different configurations of the integers.

##### 1. Weak coupling $\gamma \ll 1$

Let us begin by considering the weak coupling limit. As previously mentioned, for the ground state configura-

(a)  $\gamma = 0.1$



(b)  $\gamma = 0.5$

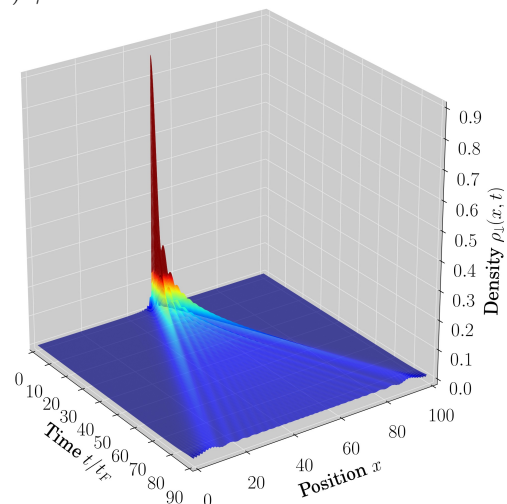


FIG. 2. **Fermions:** Time-evolution of the density profile of the minority species  $\rho_\downarrow(x, t)$  for the exciton-like state (13) with  $N = 100$  fermions on the length  $L = 100$  ring and interaction parameter (a)  $\gamma = 0.1$ ; (b)  $\gamma = 0.5$ . The configuration of integers  $\{I\}$  is the ground state ‘Fermi sea’ and we rescale the time axis by the Fermi time  $t_F = 1/\pi^2$ .

tion of integers (14), we can interpret the state as a linear superposition of spin wave excitations. At weak coupling, the spin wave velocity at small momentum  $p \ll \varrho$  is given by [104]

$$v_s = 2p \left( 1 - \frac{\gamma^2}{\pi^4} \right) + O(\gamma^3). \quad (20)$$

Accordingly, up to small differences in the initial state configuration, we should expect the nonequilibrium dynamics of the system at small  $\gamma$  to be essentially interaction-independent. As an example, in Fig. 2 we show the time-evolution of the minority density for  $\gamma =$

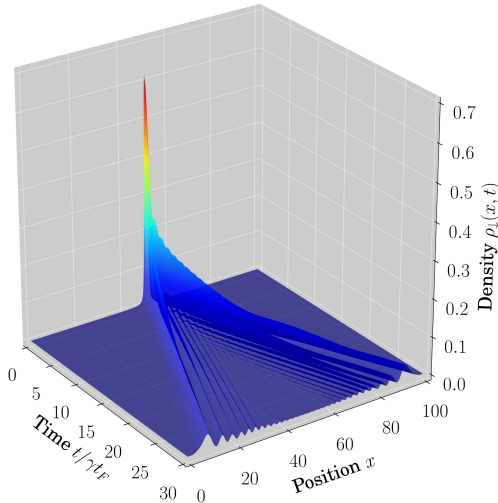
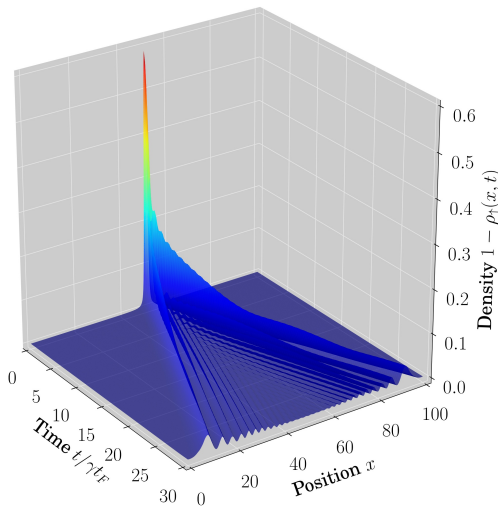
(a) Minority species  $\sigma = \downarrow$ (b) Majority species  $\sigma = \uparrow$ 

FIG. 3. **Fermions:** Time-evolution of the density profile of (a) the minority species  $\rho_{\downarrow}(x, t)$ ; (b) the hole in the majority species  $1 - \rho_{\uparrow}(x, t)$  for the exciton-like state (13) with  $N = 100$  fermions on the length  $L = 100$  ring and interaction parameter  $\gamma = 50$ . The configuration of integers  $\{I\}$  is the ground state ‘Fermi sea’ and we rescale the time axis by the Fermi time  $\gamma t_F = \gamma/\pi^2$ .

0.1, 0.5 in a system with  $N = 100$  particles on the length  $L = 100$  ring. We see that indeed the time-evolution is very similar; in both cases, by the time excitations reach the boundaries, the density within the light cone is almost constant – the exciton has completely dissolved.

## 2. Strong coupling $\gamma \gg 1$

Now we turn our attention to the strong coupling regime  $\gamma \gg 1$ . In Fig. 3 we present the time-evolution of the densities (19) starting from the initial state (13)

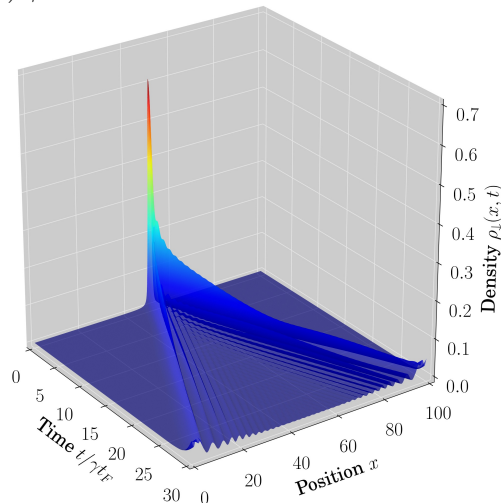
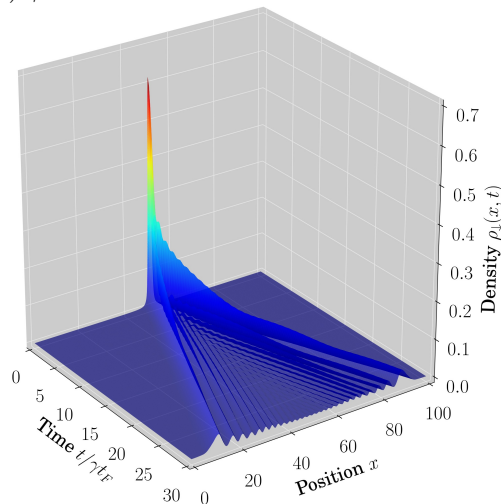
(a)  $\gamma = 100$ (b)  $\gamma = 25$ 

FIG. 4. **Fermions:** Time-evolution of the density profile  $\rho_{\downarrow}(x, t)$  for  $N = 100$  fermions on the length  $L = 100$  ring with interaction strength (a)  $\gamma = 100$ ; (b)  $\gamma = 25$ . The configuration of integers in the initial state (13) is the ground state ‘Fermi sea’. We rescale the time axis by  $\gamma t_F$  and observe the (approximate) collapse of data for both cases; compare also to Fig. 3(a) for  $\gamma = 50$ . Similar collapse is observed for  $\rho_{\uparrow}(x, t)$ .

with the ground state configuration of integers  $\{I\}_0$  for  $N = 100$  particles at unit filling  $\varrho = 1$  with interaction parameter  $\gamma = 50$ . The time axis is rescaled by  $\gamma$  and the Fermi time  $t_F = 1/E_F = 1/(\varrho\pi)^2$ ; we see that (at fixed  $N, L$ ) the results approximately collapse for different interaction strengths  $\gamma$  under such a rescaling, see Fig. 4.

Under time-evolution the exciton delocalizes, with particle-hole excitations spreading through the system at a number of different velocities, the fastest velocity defining an obvious light cone. The observed behavior,

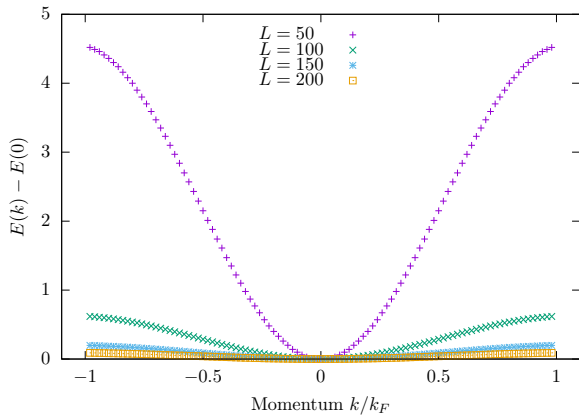


FIG. 5. The dispersion relation for the states in the superposition (13) for  $N = 100$  fermions with interaction parameter  $c = 50$  for a number of system sizes. The momentum is rescaled by the Fermi momentum  $k_F = \pi\varrho \equiv \pi N/L$ .

as well as the collapse of data upon rescaling the time-axis by  $\gamma t_F$ , can be understood in the following manner. The initial state (13) is a linear superposition of spin wave excitations [105]. These spin wave excitations have momentum  $p$  determined by the integers  $\{I\}$  and  $J$  of each state in superposition (13) through Eq. (7). In the strong coupling limit  $\gamma \gg 1$ , the velocity of a spin wave excitation with momentum  $p \ll \varrho$  is known [104]

$$v_s = 2p \left( \frac{1}{N} + \frac{2\pi^2}{3\gamma} \right) + O(\gamma^{-2}). \quad (21)$$

For the large number of particles we consider  $N \gg \gamma/\pi^2$  and hence the first term in the bracket is negligible. Accordingly, the time  $t_*$  it takes for a spin excitation of momentum  $p$  to travel unit distance is

$$t_* = \frac{1}{v_s} \approx \frac{3\gamma}{4\pi^2 p}, \quad (22)$$

and hence  $t_*/\gamma t_F = 3\varrho^2/4p$  is interaction-independent. This is the origin of the approximate data collapse at fixed  $\varrho$  with different interaction strengths  $\gamma$  upon rescaling.

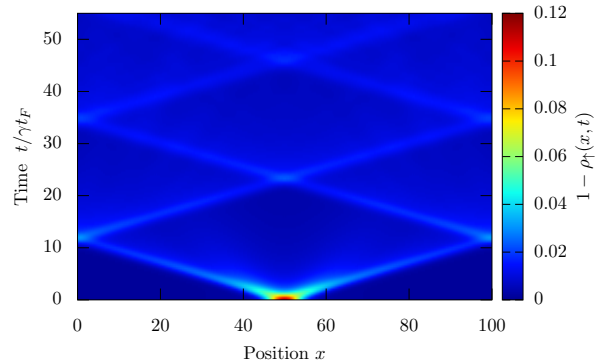
The result (22) also gives some insight in to the observed spreading of the density: the light cone is governed by high momentum  $p$  spin waves contained in the initial state (13), with lower momentum modes propagating more slowly through the gas (observed as oscillations within the light cone, see Fig. 3 and Fig. 4). Similar behavior is seen when  $\gamma$  is varied through changing the system size  $L$ , with fixed particle number  $N$  and interaction parameter  $c$ , see Appendix A. We can check that this picture gives the correct intuition (away from  $p \ll \varrho$ , where Eq. (21) applies) by plotting the energy-momentum relation for the states entering the superposition (13); this reveals the full dispersion for the spin wave excitations in the initial state (13) of the Fermi gas. We show this relation in Fig. 5; indeed high momentum modes govern the

light cone, although states with momentum close to the Fermi momentum move slower than those with  $p \sim k_F/2$ .

### 3. Other configurations of the integers $\{I\}$

Having discussed in detail the case of the ground state configuration of integers  $\{I\}_0$ , let us now consider the non-equilibrium dynamics of the initial state (13) with the diluted Fermi sea  $\{I\}_d$  and the shifted Fermi sea  $\{I\}_s$  of integers, see Eqs. (15) and (16) respectively. In Fig. 6 we present an example of the dynamics with the diluted Fermi sea of integers (15). The initial state now contains both a superposition of spin wave excitations and numerous charge excitations (corresponding to the particle/hole excitations in the integers  $\{I\}$ ). We see that the initial localized density excitation dissolves, with excitations propagating out within a light cone. The excitations in the Fermi gas propagate at almost twice the speed of those in the ground state configuration of integers (14), which is natural as the momentum of the spin waves should be approximately doubled (approximately doubling their velocity).

(a) Majority species  $\sigma = \uparrow$



(b) Minority species  $\sigma = \downarrow$

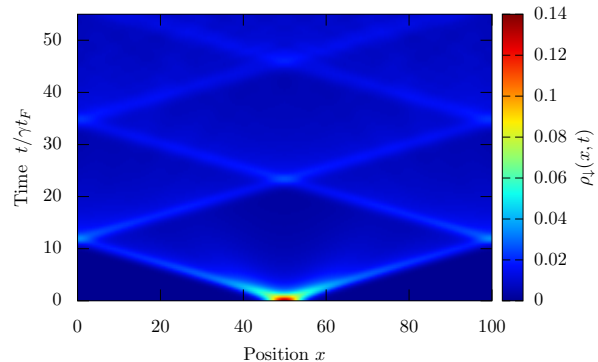


FIG. 6. **Fermions:** Here we present an example of the non-equilibrium time-evolution of the initial state (13) with the diluted Fermi sea of integers (15) for (a)  $\sigma = \uparrow$  fermions; (b)  $\sigma = \downarrow$  fermions. We consider  $N = 100$  particles on the length  $L = 100$  ring with interaction parameter  $\gamma = 10$ .

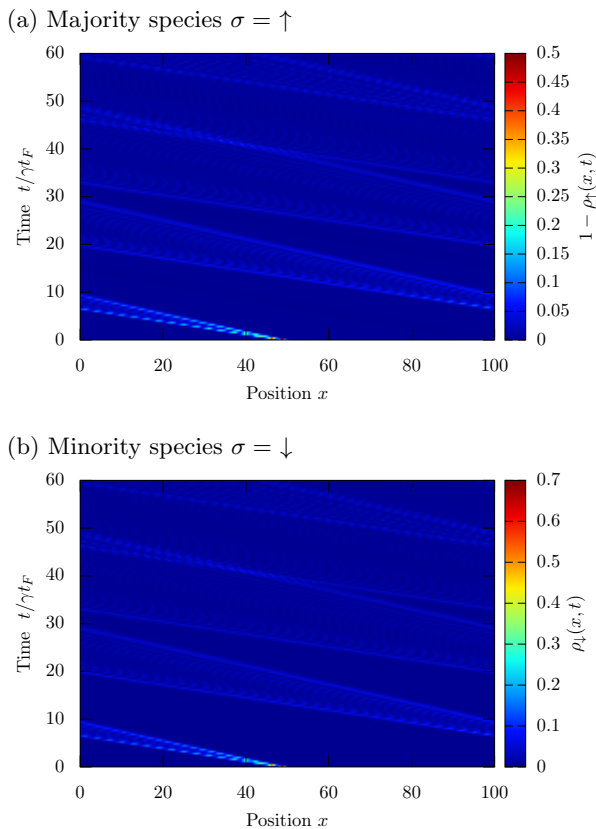


FIG. 7. **Fermions:** Here we present an example of the non-equilibrium time-evolution of the initial state (13) with the shifted Fermi sea of integers (16) for (a)  $\sigma = \uparrow$  fermions; (b)  $\sigma = \downarrow$  fermions. We consider  $N = 100$  particles on the length  $L = 100$  ring with interaction parameter  $\gamma = 10$ .

Figure 7 shows the non-equilibrium dynamics of the shifted Fermi sea of integers (16) initial state (13). We see that the initially well-localized density configuration moves rapidly to the left whilst slowly delocalizing. By time  $t \sim 10t_F$ , the localized wave packet has propagated around the ring; this repeats with the wave packet delocalizing more as time progresses. The spreading of the wave packet is clearly suppressed in comparison to the ground state configuration (14), see Fig. 3. This is quite natural – if we think of the spin wave dispersion, Fig. 5, the spreading of the wave packet is now governed by the difference in velocity between the fastest and slowest left-moving spin wave excitations. Compare this to the difference in velocity between the fastest left-moving and fastest right-moving modes which governs the spreading of the ground state configuration of integers  $\{I\}_0$ , see Fig. 3, and we naturally get a suppression of the spreading in the shifted Fermi sea case.

### III. BOSONS

#### A. The Yang-Gaudin Bose gas

Having considered the nonequilibrium dynamics of the initial state (13) in the Yang-Gaudin Fermi gas, we now turn our attention to the Yang-Gaudin Bose gas. We consider the Hamiltonian (1) with bosonic fields  $\Psi_\sigma(x)$  which obey the canonical commutation relations

$$\left[ \Psi_\sigma(x), \Psi_{\sigma'}^\dagger(y) \right] = \delta_{\sigma, \sigma'} \delta(x - y). \quad (23)$$

The index  $\sigma = \uparrow, \downarrow$  labels a pseudo spin-1/2 degree of freedom: in the context of experiments on cold atomic gases, it may label two hyperfine states [65, 113] or two different species of atoms [68].

##### 1. Solution via the Bethe ansatz

As with the Fermi gas, the Bose gas is exactly solvable [51, 88]; an  $N$ -particle eigenstate  $|\{k\}; \{\nu\}\rangle$  which contains  $M$  down bosons is characterized by two sets of quantum numbers:  $N$  quasi-momenta  $\{k\} \equiv \{k_1, \dots, k_N\}$  and  $M$  spin rapidities  $\{\nu\} \equiv \{\nu_1, \dots, \nu_M\}$ . These sets satisfy the logarithmic Bethe ansatz equations (*cf.* Eqs. (3)) [51, 88]

$$\begin{aligned} 2\pi I_i &= k_i L - \sum_{\alpha=1}^M \phi_2(k_i - \nu_\alpha) + \sum_{l=1}^N \phi_1(k_i - k_l), \\ 2\pi J_\alpha &= \sum_{l=1}^N \phi_2(\nu_\alpha - k_l) - \sum_{\beta=1}^M \phi_1(\nu_\alpha - \nu_\beta), \end{aligned} \quad (24)$$

where the scattering phase is defined as in the Fermi gas, *i.e.*,

$$\begin{aligned} \phi_n(u) &= i \log \left( \frac{\frac{ic}{n} + u}{\frac{ic}{n} - u} \right), \\ &\equiv 2 \arctan \left( \frac{un}{c} \right), \end{aligned} \quad (25)$$

see Eq. (4).  $\{I\} \equiv \{I_1, \dots, I_N\}$  and  $\{J\} \equiv \{J_1, \dots, J_M\}$  are sets of ‘integers’ satisfying

$$I_i, J_\alpha \in \begin{cases} \mathbb{Z} & \text{if } (N + M) \in 2\mathbb{Z} + 1, \\ \mathbb{Z} + \frac{1}{2} & \text{if } (N + M) \in 2\mathbb{Z}. \end{cases} \quad (26)$$

The sets of integers obey an exclusion principle:  $I_i \neq I_j$  for  $i \neq j$  and  $J_\alpha \neq J_\beta$  for  $\alpha \neq \beta$ . The eigenstate  $|\{k\}; \{\nu\}\rangle$  has energy  $E_{\{k\}}$  and momentum  $P_{\{k\}}$  given in terms of the quasi-momenta by Eq. (8) and Eq. (7), respectively. The ground state configuration of the integers  $\{I\}$  is a ‘Fermi sea’ about the origin [114]. The scattering phase (4) is bounded  $|\phi_n(u)| \leq \pi/2$  and hence so are the integers  $|J_\alpha| \leq (N + M)/2$ . An analogous restriction applies in the one-dimensional Hubbard model [93]. The integrability of the model is realized in the constants of motion  $\mathcal{I}_n = \sum_{j=1}^N k_j^n$  where  $n \in \mathbb{N}$ .

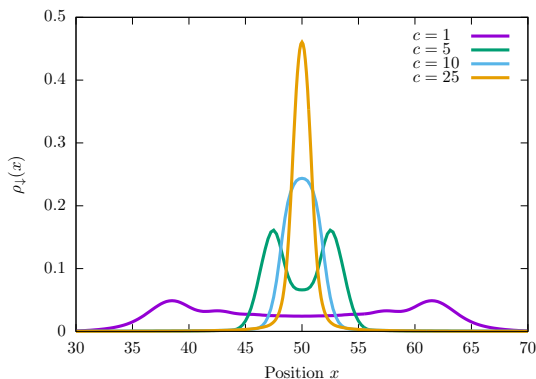


FIG. 8. **Bosons:** The minority density profile  $\rho_{\downarrow}(x) = \langle \Psi_{\downarrow}^{\dagger}(x)\Psi_{\downarrow}(x) \rangle$  for the exciton-like initial state  $|\{I\}\rangle$ , see Eq. (13). We have considered the ground state configuration of the integers  $\{I\}_0$ . Data is presented for  $N = 100$  particles at unit filling for a number of interaction strengths:  $c = 1, 5, 10, 25$ . Overlap of the initial state with a simple spin flip excitation (18) are shown in Table II.

## 2. Known properties

Equilibrium properties of the Yang-Gaudin Bose gas are relatively well understood [61]; at zero-temperature there is a well-known theorem that the ground state of a two-component Bose gas with spin-independent interaction is spin-polarized [100, 101]. This can be seen from the Bethe ansatz solution [115, 116]; these techniques can also be extended to finite-temperature and used to study the temperature-dependent polarization [117] and other thermodynamic quantities [118], as well as to the case of inhomogeneous systems [119]. Excitations above the zero-temperature spin-polarized ground state have also been studied using the coordinate Bethe ansatz [105, 116]. At strong coupling, unusual logarithmic diffusion was observed in the spin-flip dynamical correlation functions due to the large effective mass for spin waves [105, 106]. Out of equilibrium, much less is understood; progress has been hampered by lack of knowledge of matrix elements, although for small numbers of particles  $N \sim 10$  the dynamics of a Gaussian impurity has been studied [85].

## B. The exciton-like initial state

### 1. Density profile of the exciton-like state

We now turn our attention to the initial state (13) constructed within the Yang-Gaudin Bose gas. We present the impurity density profile

$$\rho_{\downarrow}(x) = \langle \{I\} | \Psi_{\downarrow}^{\dagger}(x)\Psi_{\downarrow}(x) | \{I\} \rangle, \quad (27)$$

composed with the ground state configuration [114] of integers  $\{I\}_0$  in Fig. 8. We are limited to examining

$\gamma$	$QL/2\pi$	Overlap $ \mathcal{C} $
1	2	0.2002
5	4	0.2926
10	5	0.3353
25	6	0.3573
50	6	0.3621
100	6	0.3640
500	6	0.3653

TABLE II. **Bosons:** Overlap of the initial state (13) with the localized spin flip excitation (18) in the Yang-Gaudin Bose gas with momentum  $Q$ , chosen to maximize the overlap. We choose  $|\Omega\rangle$  to be the one-component state with the Fermi sea of integers shifted one position to the left relative to the ground state. The shape of the spin flip excitation,  $f(x)$  in Eq. (18), is chosen to reproduce the density of the impurity, see Fig. 8. Here we use  $N = L = 30$ . The computed overlap is only weakly dependent on the system size at fixed density.

the impurity sector  $\sigma = \downarrow$ , as an efficient representation for matrix elements of the majority density are currently not known to us, *cf.* Ref. [58]. We see a similar qualitative picture (with much more drastic  $c$ -dependence) to the fermionic case, *cf.* Fig. 1; there is a single well-localized density configuration for the impurity when  $c$  is large. For small and intermediate strengths of the interaction, the impurity delocalizes to a larger extent than the fermionic case. By analogy with the Fermi gas, we expect there to be a well-localized hole in the background gas, forming an exciton-like configuration. Our data is presented for  $N = 100$  particles at unit density  $\rho = 1$ .

### 2. Overlap with spin-flip excitation

As with the fermionic case, see Sec. II C 2, we consider the overlap of the initial state (13) with a simple spin flip excitation (18). In Table II we present the overlap for a range of interaction strengths; once again, we see that the initial state (13) has a considerable overlap with simple spin flip states which may be prepared experimentally [65].

### 3. Other configurations of the integers $\{I\}$

We are not limited to studying the ground state configuration of integers  $\{I\}_0$ ; we can consider any configuration. As with the fermions, we will also consider (*cf.* Eqs. (15–16)):

1. The ‘diluted Fermi sea’, where every other integer is filled

$$\{I\}_d = \{-N, -N + 2, \dots\}. \quad (28)$$

2. The ‘shifted Fermi sea’, where we construct a

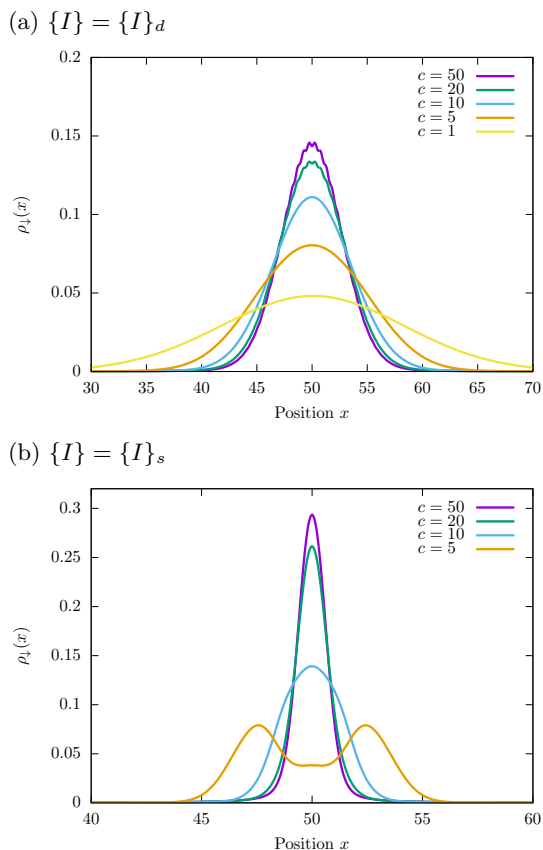


FIG. 9. **Bosons:** The density  $\rho_{\downarrow}(x, t)$  for the initial state (13) with (a) the diluted Fermi sea of integers  $\{I\}_d$ , see Eq. (28); (b) the shifted Fermi sea of integers, see Eq. (29). We consider  $N = 100$  particles on the length  $L = 100$  ring for a number of interaction strengths  $c$  (labelled). *cf.* Fig. 8 for the ground state configuration of integers  $\{I\}$ .

‘Fermi sea’ with, e.g., the negative integers:

$$\{I\}_s = \{-N + 1, -N + 2, \dots, 0\}. \quad (29)$$

In Fig. 9 we present the initial state density for  $N = 100$  bosons on the length  $L = 100$  ring for both the configurations of integers introduced above. For the diluted Fermi sea, Eq. (28), we see that there are some significant changes when compared to the ground state configuration, see Fig. 8. Firstly, at small interaction strengths the multiple peak structure is removed, whilst for large interactions the peak has broadened and reduced in height. Additionally, for strong interactions there are small amplitude oscillations superimposed on the main peak structure. The state described by the diluted Fermi sea of integers is now rather complicated – as well as containing a superposition of spin wave excitations, there are also numerous  $N/2$  charge excitations within each state. For the shifted Fermi sea of integers, Eq. (29), the  $t = 0$  behavior is reminiscent of the ground state configuration with some additional broadening of the peak structure.

### C. Non-equilibrium dynamics of the exciton-like state

We now turn our attention to the time-evolution of the initial state (13) in the Yang-Gaudin Bose gas. We study the expectation values of the ‘impurity’  $\sigma = \downarrow$  density operator [120]

$$\rho_{\downarrow}(x, t) = \langle \{I\} | e^{iHt} \Psi_{\downarrow}^{\dagger}(x) \Psi_{\downarrow}(x) e^{-iHt} | \{I\} \rangle, \quad (30)$$

which we compute by the matrix element expansion described in Sec. II B.

#### 1. Weak coupling $\gamma \ll 1$

At weak coupling, the effective mass of the spin wave  $m_*$  with small momentum  $p \ll \rho$  is given by [105, 121]

$$\frac{m}{m_*} = 1 - \frac{2\sqrt{\gamma}}{3\pi}, \quad (31)$$

which shows that correlations between the particles gives rise to non-analytic corrections to the bare spin wave mass. Notice that the interaction corrections to the bare mass are much stronger for the Yang-Gaudin Bose gas than the Fermi gas, *cf.* Eq. (20). The weak coupling spin wave dynamics do not coincide for bosons and fermions. We will not discuss further the weak coupling case of the bosons, as the initial density profile, see Fig. 8, is far from well-localized and the picture of spin wave excitations emerging from a point and propagating clearly does not hold. The shape of the impurity can be partially sharpened up by choosing a different configuration of the integers  $\{I\}$ , see Sec. III B 3.

#### 2. Strong coupling $\gamma \gg 1$

Let us now consider the strong coupling regime  $\gamma \gg 1$ . We present data for a system of  $N = 100$  boson on the length  $L = 100$  ring with interaction parameters  $\gamma = 25, 50$  in Fig. 10, where we choose the ground state configuration of integers  $\{I\}_0$  [120]. As with the fermionic case, we see that the two cases collapse on to one another after rescaling the time axis by  $\gamma t_F$ . The origin of this is the same as with the fermions, see Eq. (21) and Eq. (22); the spin velocity in the  $\gamma \gg 1$  limit of the Bose gas and the Fermi gas coincide [105, 121] (this is not surprising, as the bosons ‘fermionize’ at  $\gamma = \infty$ , obeying a hardcore exclusion principle).

There are, however, differences between the Fermi gas and the Bose gas. Noticeably, the oscillations in the Bose gas are much less ‘clean’ than the Fermi gas (*cf.* Fig. 3) as the result of there being two prominent light cones, revealed much more clearly when the density is varied, see Fig. 11. The second prominent light cone behaves very differently to the leading front: the excitations propagate

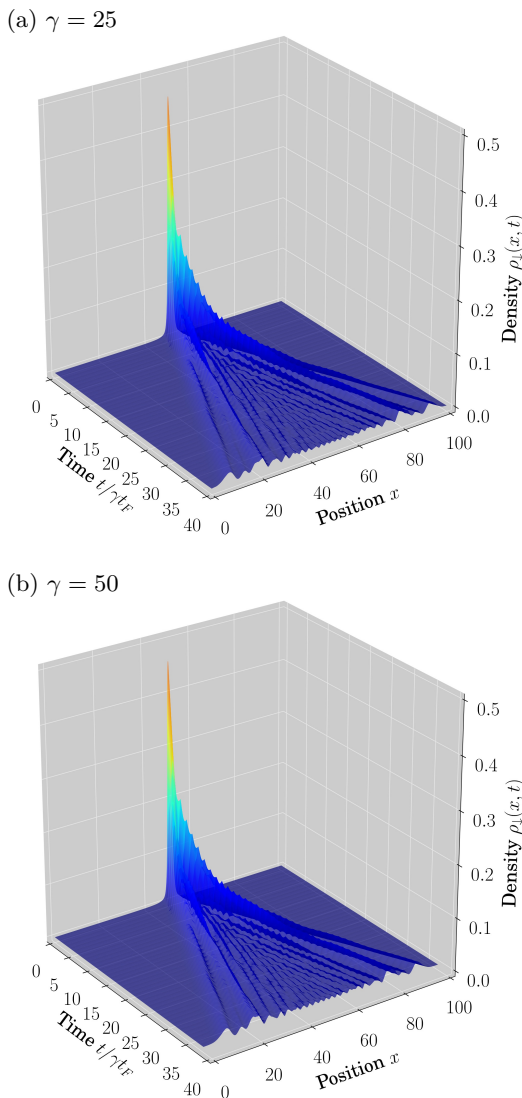


FIG. 10. **Bosons:** Time-evolution of the density profile  $\rho_{\downarrow}(x,t) = \langle \{I\} | \Psi_{\downarrow}^{\dagger}(x,t) \Psi_{\downarrow}(x,t) | \{I\} \rangle$  for  $N = 100$  bosons at unit filling with dimensionless interaction parameter (a)  $\gamma = 25$ ; (b)  $\gamma = 50$ . The set of integers  $\{I\}$  is the ground state ‘Fermi sea’ configuration. Rescaling the time-axis by  $\gamma t_F = \gamma/\pi^2$  results in the two cases ‘collapsing’ on to one another.

through the gas in a manner not taken into account by the  $t \rightarrow t/\gamma t_F$  rescaling when the system size is varied.

What is the origin of this ‘slow mode’ within the leading light cone? To start, we can rule out two scenarios: (i) low momentum spin wave excitations  $p \ll \varrho$  with velocity (21); (ii) ‘charge excitations’ moving with the Fermi velocity  $v_F \approx 2\pi\varrho$ . In both cases, it is easy to show that the time it takes for the excitations to propagate distance  $L/2$  does not scale in the same manner as that observed for the ‘slow mode’.

Having ruled out low-momentum spin wave excitations and charge excitations, we can gain some insight into

the ‘slow mode’ by studying the full spin wave dispersion relation by computing the energy and momentum of each state in the superposition (13) through Eqs. (8) and (7). In Fig. 12 we show the dispersion relation for  $N = 100$  bosons with interaction  $c = 50$  on the  $L = 50-200$  length ring (*cf.* Fig. 11), which should be compared to Fig. 5 for the Fermi gas. We see that there are rather dramatic differences between the states for bosons and fermions, and it is this difference which is the origin of the ‘slow mode’.

Firstly, if we restrict our attention to states with momentum  $|k| \leq k_F$ , we see that the two cases look very similar, as is to be expected at strong coupling. However, focusing on the initial state (13) for bosons, spin wave excitations extend to momentum  $|k| \leq 2k_F$  – this is a result of the rules for the quantum numbers (26) which lead to two choices for the Fermi sea (see [114]) satisfying  $|\sum_j I_j| = N/2$ . As a result, the maximal value of the momentum of a state (7) is  $|P_{\{k\}}| \leq 2k_F$ , rather than  $k_F$  as for fermions [114].

Let us define the spin wave velocity through the relation

$$v_s = \frac{dE_J}{dP_J}, \quad (32)$$

where  $E_J, P_J$  are the energy and momentum of the state with spin rapidity integer  $J$  in the superposition (13). We show the spin velocity for excitations with momentum  $k$  in Fig. 13. We see that there are two ‘major’ propagation velocities in the system,  $v_{s,1}$  corresponding to the cluster of states with momentum  $|k| \sim k_F/2$  and  $v_{s,2}$  corresponding to states with momentum  $|k| \sim 3k_F/2$ . For clarity, we label these velocities explicitly in Fig. 13. The ratio of these two propagation velocities varies with the system size  $L$ , which has important implications for the ‘slow mode’. For the reported data, we have  $v_{s,2}/v_{s,1} \approx 0.7$  when  $L = 50$  which drops to  $v_{s,2}/v_{s,1} \approx 0.2$  when  $L = 200$ . This is consistent with the behavior of the ‘slow mode’ seen in Fig. 11; the ‘slow mode’ becomes increasingly slower when compared to the leading light cone with increasing system size. Thus, we propose that excitations about the roton-like minima in the dispersion, Fig. 12, which correspond to the velocity  $v_{s,2}$  in Fig. 13, are the origin of the ‘slow mode’ observed in the time-evolution of the bosonic initial state (13). This roton-like minima in the spin wave dispersion was noted in Ref. [116] and persists to small values of the interaction parameter  $c \sim 1$ .

### 3. Other configurations of the integers

Finally, we consider the non-equilibrium dynamics of the initial state (13) for bosons constructed with two other distributions of the integers  $\{I\}$ , the diluted Fermi sea (28) and the shifted Fermi sea (29).

In Fig. 14, we present the nonequilibrium dynamics with the diluted Fermi sea; the state now contains both

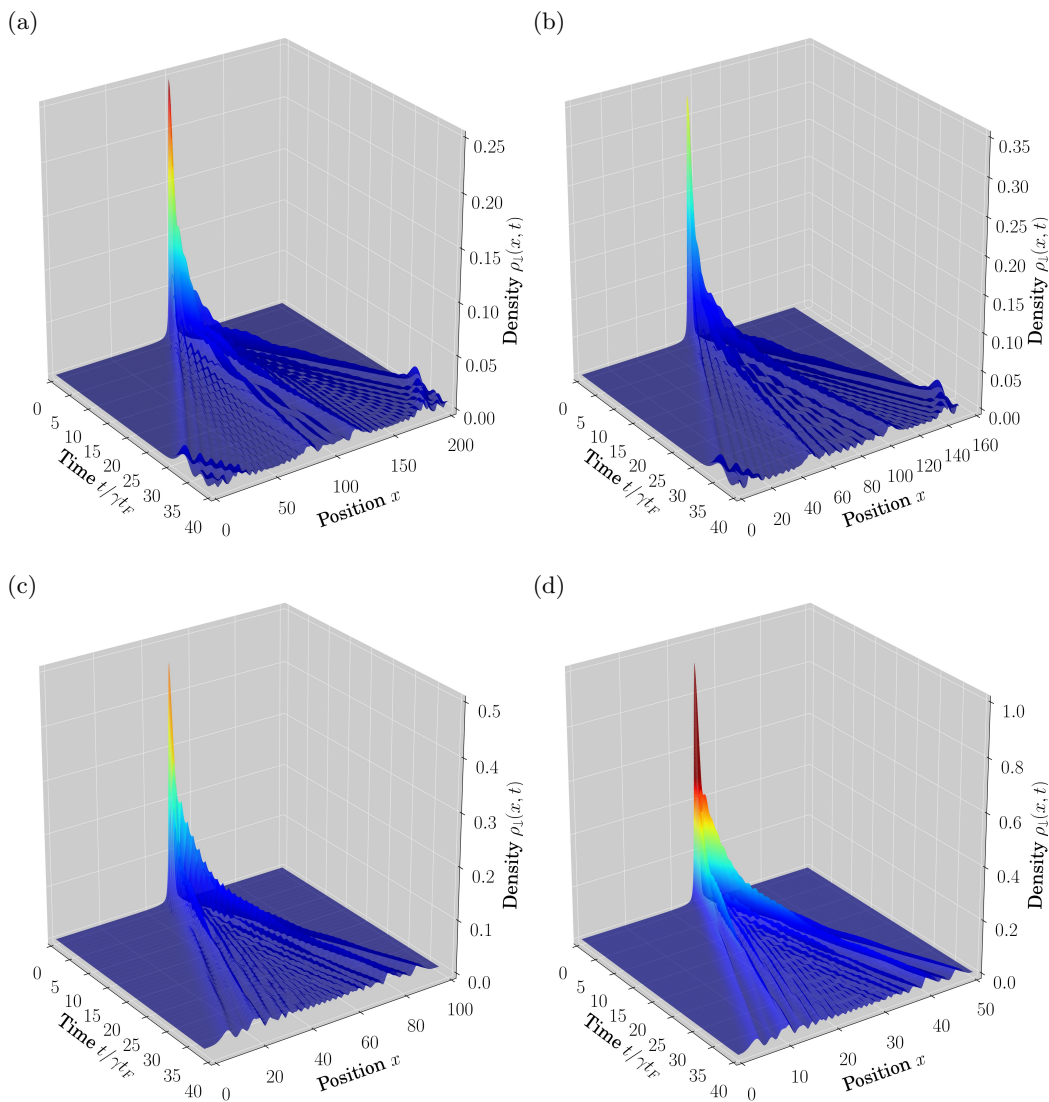


FIG. 11. **Bosons:** We trace how the time-evolution of the density profile  $\rho_{\downarrow}(x, t) = \langle \{I\} | \Psi_{\downarrow}^{\dagger}(x, t) \Psi_{\downarrow}(x, t) | \{I\} \rangle$  evolves with changing the system size  $L$  with fixed numbers of particle  $N = 100$  and interaction parameter  $c = 50$ . The ground state configuration of the integers  $\{I\}$  is considered. Data is presented for (a)  $L = 200$  ( $\gamma = 100$ ); (b)  $L = 150$  ( $\gamma = 75$ ); (c)  $L = 100$  ( $\gamma = 50$ ) and (d)  $L = 50$  ( $\gamma = 25$ ). The time axis is rescaled by  $\gamma t_F = c/(\varrho^3 \pi^2)$ . A pronounced ‘slow mode’ is observed with dilution of the system.

spin wave excitations and numerous charge excitation (corresponding to particle-hole excitation of the Fermi sea of integers, see Sec. II A 3). The initial configuration, containing a localized density configuration as shown in Fig. 9, dissolves with excitations propagating out within a light cone. The light cone splits into a double peak structure after  $t \sim 30t_F$ , unlike the Fermi gas (see Fig. 6). This is reminiscent of the double peak structure in Fig. 10, which is the result of the spin wave roton-like excitation.

The shifted Fermi sea of integers (29) also begins with a localized density excitation, as seen in Fig. 9. Due to the shifting of the Fermi sea of integers (29), the state now carries an average center of mass momentum; the

localized density propagates to the left and spreads. The spreading of the peak is clearly suppressed when compared to the ground state configuration, see Figs. 10 and 11. As with the discussion of the fermions, see Sec. II D 3, this is a natural expectation.

#### IV. CONCLUSIONS

In this work we have investigated the nonequilibrium dynamics of a class of exciton-like initial states (13) which can be constructed in two-component integrable quantum gases. Focusing on the ground state configuration of integers  $\{I\}_0$ , these states can be pictured as a lin-

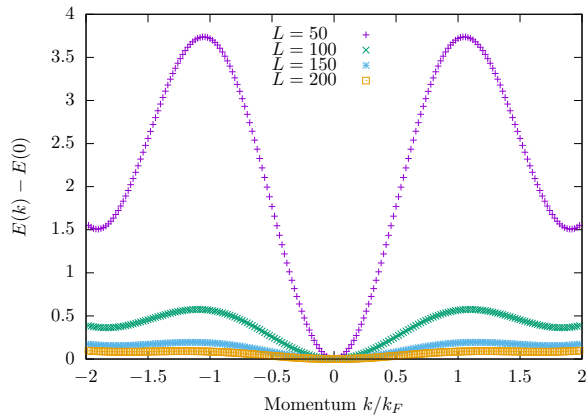


FIG. 12. The dispersion relation for the states in the superposition (13) for  $N = 100$  bosons with interaction parameter  $c = 50$  for a number of system sizes. The momentum is rescaled by the Fermi momentum  $k_F = \pi \rho \equiv \pi N/L$  and we measure the energy relative to  $E(0)$ , corresponding to the configuration of integers  $I = \{-N/2, \dots, -N/2 + 1\}$ ,  $J = -N/2$ . *cf.* Ref. [116].

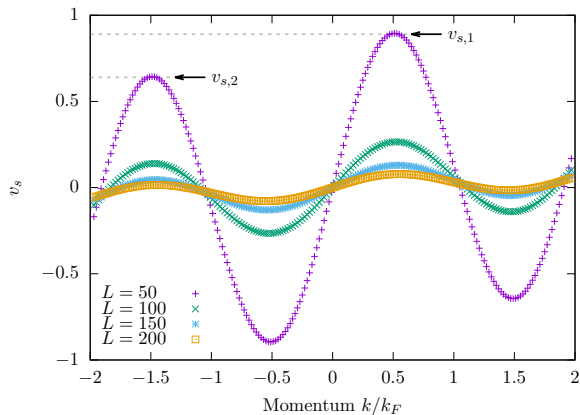


FIG. 13. **Bosons:** The velocity  $v_s$  of spin wave excitations with momentum  $k$  in a system of  $N = 100$  boson with interaction parameter  $c = 50$  for a number of system sizes  $L$ . The momentum is rescaled by the Fermi momentum  $k_F = \pi \rho \equiv \pi N/L$ . For the  $L = 50$  data we explicitly highlight the peak velocities  $v_{s,1}$  and  $v_{s,2}$  discussed in the text.

ear superposition of spin wave excitations and they have significant overlap with realistic ‘spin flip’ states (18). The superposition of spin waves with different momentum  $p$ , leads to a single well-localized particle-hole density configuration, looking much like an exciton. The simple structure of this class of states means that the time-evolution can be computed for large numbers of particles  $N \sim 100 - 1000$  (see Appendix B), comparable to those studied in experiments [65]. Additionally, summation of matrix elements required for the time-evolution is *numerically exact*, with no need for truncation or approximations.

Under time-evolution, the initially well-localized

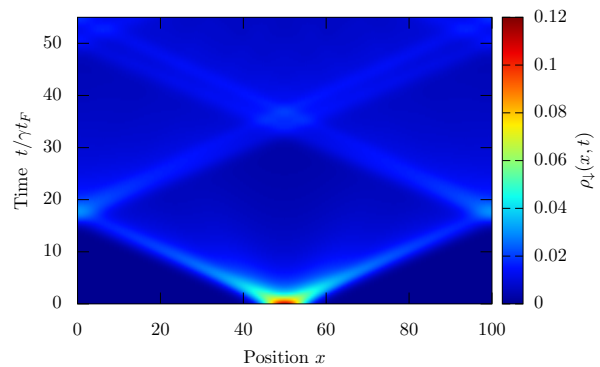


FIG. 14. **Bosons:** Here we present an example of the non-equilibrium time-evolution of the initial state (13) with the diluted Fermi sea of integers (15) for  $\sigma = \downarrow$  bosons. We have considered  $N = 100$  particles on the length  $L = 100$  ring with interaction parameter  $\gamma = 10$ .

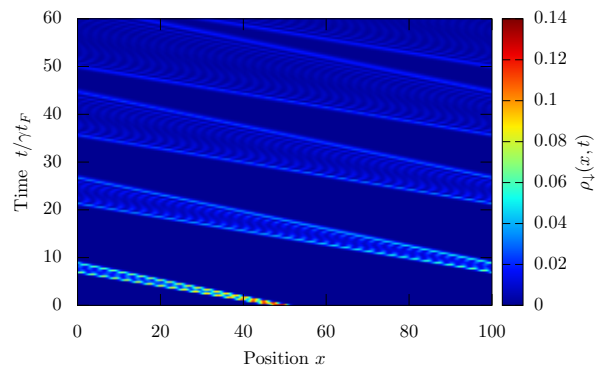


FIG. 15. **Bosons:** Here we present an example of the non-equilibrium time-evolution of the initial state (13) with the shifted Fermi sea of integers (29) for  $\sigma = \downarrow$  bosons. We have considered  $N = 100$  particles on the length  $L = 100$  ring with interaction parameter  $\gamma = 10$ .

exciton-like configuration dissolves, with particle-hole excitations spreading through the gas within a light cone. The leading edge of the light cone is due to high momentum spin waves in the initial state (13); lower momentum modes propagate more slowly and appear within the light cone (see Fig. 3 and Fig. 10). When interactions are strong, the time-evolution of the density for different interaction strengths collapses upon rescaling the time  $t \rightarrow t/\gamma t_F$ , which can be understood from the strong coupling expansion of the spin wave velocity (21). For weak interactions, the dynamics are independent of  $\gamma$  for sufficiently weak interactions (which are much smaller for bosons than fermions, compare Eqs. (20) and (31)).

A prominent difference between the Fermi gas and the Bose gas is the appearance of a ‘slow mode’ upon varying the system size in the Bose gas at strong coupling. Simple scaling arguments rule out this ‘slow mode’ being associated with low-momentum spin wave excitations or low-energy density excitations (with velocity close to the

Fermi velocity). We have presented evidence that the ‘slow mode’ is a signature of excitations about a (finite momentum) roton-like minimum in the spin wave dispersion [116]. These spin wave roton-like excitations of the Yang-Gaudin gas should be the subject of future investigations, as there may be interesting implications for finite-temperature properties of the Yang-Gaudin Bose gas, as well as other nonequilibrium dynamics.

The special structure of the initial state (13), which can be interpreted as a superposition of spin wave excitations on top of a background gas defined by the integers  $\{I\}$ , does have some important consequences. We do not see any evidence of ‘quantum stutter’ behavior [85]; the quadratic dispersion at small momenta means that spin wave excitations are essentially free (with an interaction-dependent effective mass) to propagate through the background gas. Whilst the state (13) will have some small overlap with the initial state considered in Ref. [85], a large number of states with different distributions of integers is required to capture the physics there, and scattering between different types of excitations in the system (e.g., different configurations of the integers  $\{I\}$  and  $J$ ) is clearly important.

We have also explored some of the flexibility offered by the class of initial states (13) and we present data for other configurations of the integers  $\{I\}$ ; we focused on two particular choices: the ‘diluted Fermi sea’ and the ‘shifted Fermi sea’. Ultimately, the nonequilibrium time-evolution of the initial state with the diluted Fermi sea of integers  $\{I\}_d$  is very similar to the ground state configuration. The leading edge of the light cone with  $\{I\}_d$  travels approximately twice as fast as the case with  $\{I\}_0$ , reflecting the fact that the momentum of the spin waves

is doubled. With the shifted Fermi sea of integers  $\{I\}_s$ , the state now has a finite center of mass momentum and the initially localized exciton-like configuration moves as it spreads.

Our study highlights the power of integrability, as well as the importance in a judicious choice of state. Our initial state has significant overlap with a simple state that can be experimentally prepared (see, e.g., Ref. [65]), but contains very few eigenstates (proportional to the number of particles studied). This simple structure, when combined with knowledge of the eigenstates and matrix elements obtained from integrability, allows us to compute the exact dynamics of a large system of particles with finite interaction strength. The results that we present are obtained with modest computational resources for numbers of particles far beyond the reach of state-of-the-art exact diagonalization.

## ACKNOWLEDGMENTS

It is a pleasure to thank Bruno Bertini for interesting and useful discussions surrounding this work. NJR thanks the Institute for Theoretical Physics, University of Amsterdam for hospitality during a visit, where part of this work was undertaken. We would also like to thank the Isaac Newton Institute, University of Cambridge, for hospitality during the final stages of this work. This work was supported by the Condensed Matter Physics and Materials Science Department, Brookhaven National Laboratory, in turn funded by the U.S. Department of Energy, Office of Basic Energy Sciences, under Contract DE-SC0012704 (NJR, RMK), and the FOM and NWO foundations of the Netherlands.

### Appendix A: Varying the system size with fixed $N$ , $c$ in the Yang-Gaudin Fermi Gas

In Fig. 16 we present additional data for how the nonequilibrium dynamics of the initial state (13) in the Yang-Gaudin Fermi gas change with system size  $L$  with fixed particle number  $N$  and interaction strength  $c$ . This should be contrasted to the Bose gas, Fig. 11, where a prominent ‘slow mode’ is visible at lower densities. The approximate collapse of data at large  $\gamma$  fails, as the  $1/N$  term in the velocity, see Eq. (21), becomes increasingly important.

### Appendix B: Example computation with very large number $N = 1000$ of particles

In this appendix we provide some sample data for very large system sizes of  $N = 500 - 1000$  particles. To begin, in Fig. 17 we present the time-evolution of the initial state (13) with the ground state configuration of integers (14) for  $N = 1000$  fermions with density  $\varrho = 1/2$  and interaction strength  $\gamma = 100$ . As expected, we see essentially the same behavior as for smaller system sizes, *cf.* Fig. 16(a). Next, we present the time-evolution of  $\rho_\downarrow(x, t)$  for  $N = 500$  bosons at unit filling and interacting strength  $\gamma = 50$  in Fig. 18. As with the fermionic case, we see the same behavior as with small system sizes, *cf.* Fig. 10(b).

---

[1] A. Polkovnikov, K. Sengupta, A. Silva, and M. Venkatachalan, “*Colloquium* : Nonequilibrium dynamics of

closed interacting quantum systems,” *Rev. Mod. Phys.* **83**, 863–883 (2011).

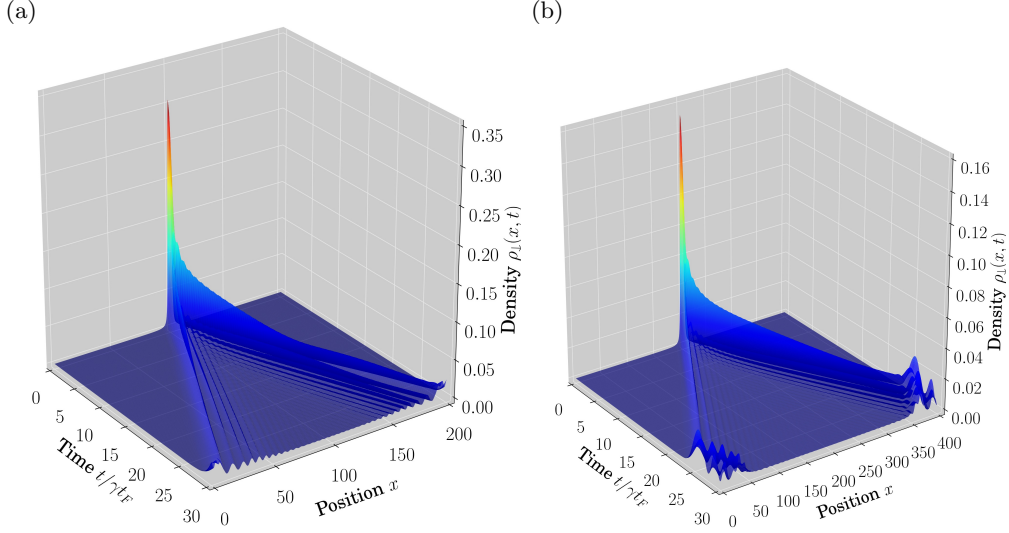


FIG. 16. **Fermions:** Time-evolution of the density profile  $\rho_{\downarrow}(x, t)$  for  $N = 100$  fermions on the length (a)  $L = 200$ ; (b)  $L = 400$  ring with interaction parameter  $c = 50$  [(a)  $\gamma = 100$ ; (b)  $\gamma = 200$ ]. The configuration of integers in the initial state (13) is the ground state ‘Fermi sea’. We rescale the time axis by  $\gamma t_F$  and observe the (approximate) collapse of data for both cases; compare also to Fig. 3 for  $c = 50$ ,  $L = 100$ .

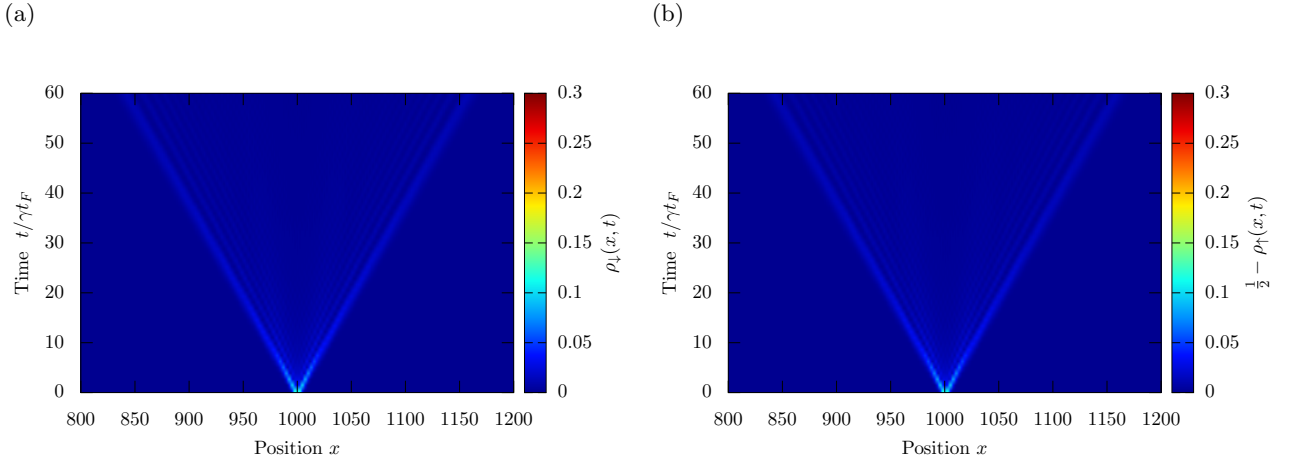


FIG. 17. **Fermions:** Time-evolution of the density profile  $\rho_{\sigma}(x, t)$  with (a)  $\sigma = \downarrow$ ; (b)  $\sigma = \uparrow$  for  $N = 1000$  fermions on the length  $L = 2000$  ring with interaction strength  $c = 50$ .

- [2] J. Eisert, M. Friesdorf, and C. Gogolin, “Quantum many-body systems out of equilibrium,” *Nature Phys.* **11**, 124–130 (2015).
- [3] L. D’Alessio, Y. Kafri, A. Polkovnikov, and M. Rigol, “From Quantum Chaos and Eigenstate Thermalization to Statistical Mechanics and Thermodynamics,” ArXiv e-prints (2015), [arXiv:1509.06411](https://arxiv.org/abs/1509.06411) [[cond-mat.stat-mech](https://arxiv.org/abs/1509.06411)].
- [4] V. E. Korepin, N. M. Bogoliubov, and A. G. Izergin, *Quantum Inverse Scattering Method and Correlation Functions* (Cambridge University Press, 1997).
- [5] M. Gaudin, *La fonction d’onde de Bethe* (Masson, 1983). English translation: M. Gaudin and J.S. Caux, *The Bethe Wavefunction* (Cambridge University Press, 2014).
- [6] P. Calabrese and J. Cardy, “Quantum quenches in extended systems,” *J. Stat. Mech.* **2007**, P06008 (2007).
- [7] P. Calabrese, F. H. L. Essler, and M. Fagotti, “Quantum quench in the transverse-field Ising chain,” *Phys. Rev. Lett.* **106**, 227203 (2011).
- [8] P. Calabrese, F. H. L. Essler, and M. Fagotti, “Quantum quench in the transverse field Ising chain: I. time evolution of order parameter correlators,” *J. Stat. Mech.* **2012**, P07016 (2012).
- [9] D. Schuricht and F. H. L. Essler, “Dynamics in the Ising field theory after a quantum quench,” *J. Stat. Mech.* **2012**, P04017 (2012).
- [10] F. H. L. Essler, S. Evangelisti, and M. Fagotti, “Dynamical correlations after a quantum quench,” *Phys. Rev. Lett.* **109**, 247206 (2012).

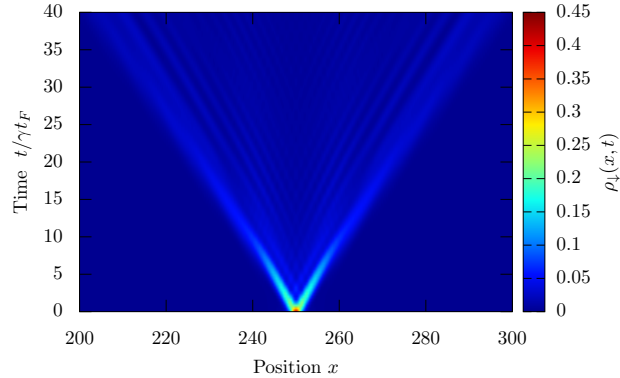


FIG. 18. **Bosons:** Time-evolution of the density profile  $\rho_{\downarrow}(x,t)$  for  $N = 500$  bosons at unit filling  $\rho = 1$  with interaction strength  $c = 50$ .

- [11] M. Collura, S. Sotiriadis, and P. Calabrese, “Equilibration of a Tonks-Girardeau gas following a trap release,” *Phys. Rev. Lett.* **110**, 245301 (2013).
- [12] J.-S. Caux and F. H. L. Essler, “Time evolution of local observables after quenching to an integrable model,” *Phys. Rev. Lett.* **110**, 257203 (2013).
- [13] M. Fagotti, “On conservation laws, relaxation and pre-relaxation after a quantum quench,” *J. Stat. Mech.* **2014**, P03016 (2014).
- [14] M. Kormos, M. Collura, and P. Calabrese, “Analytic results for a quantum quench from free to hard-core one-dimensional bosons,” *Phys. Rev. A* **89**, 013609 (2014).
- [15] M. Rigol, A. Muramatsu, and M. Olshanii, “Hard-core bosons on optical superlattices: Dynamics and relaxation in the superfluid and insulating regimes,” *Phys. Rev. A* **74**, 053616 (2006).
- [16] M. A. Cazalilla, “Effect of suddenly turning on interactions in the luttinger model,” *Phys. Rev. Lett.* **97**, 156403 (2006).
- [17] M. Rigol, V. Dunjko, V. Yurovsky, and M. Olshanii, “Relaxation in a completely integrable many-body quantum system: An *Ab Initio* study of the dynamics of the highly excited states of 1D lattice hard-core bosons,” *Phys. Rev. Lett.* **98**, 050405 (2007).
- [18] M. Cramer, C. M. Dawson, J. Eisert, and T. J. Osborne, “Exact relaxation in a class of nonequilibrium quantum lattice systems,” *Phys. Rev. Lett.* **100**, 030602 (2008).
- [19] M. Rigol, V. Dunjko, and M. Olshanii, “Thermalization and its mechanism for generic isolated quantum systems,” *Nature* **452**, 854–858 (2008).
- [20] T. Barthel and U. Schollwöck, “Dephasing and the steady state in quantum many-particle systems,” *Phys. Rev. Lett.* **100**, 100601 (2008).
- [21] M. Rigol, “Breakdown of thermalization in finite one-dimensional systems,” *Phys. Rev. Lett.* **103**, 100403 (2009).
- [22] D. Rossini, S. Suzuki, G. Mussardo, G. E. Santoro, and A. Silva, “Long time dynamics following a quench in an integrable quantum spin chain: Local versus nonlocal operators and effective thermal behavior,” *Phys. Rev. B* **82**, 144302 (2010).
- [23] D. Fioretto and G. Mussardo, “Quantum quenches in integrable field theories,” *New J. Phys.* **12**, 055015 (2010).
- [24] J.-S. Caux and R. M. Konik, “Constructing the generalized gibbs ensemble after a quantum quench,” *Phys. Rev. Lett.* **109**, 175301 (2012).
- [25] M. Fagotti and F. H. L. Essler, “Reduced density matrix after a quantum quench,” *Phys. Rev. B* **87**, 245107 (2013).
- [26] G. Mussardo, “Infinite-time average of local fields in an integrable quantum field theory after a quantum quench,” *Phys. Rev. Lett.* **111**, 100401 (2013).
- [27] B. Pozsgay, “The generalized gibbs ensemble for Heisenberg spin chains,” *J. Stat. Mech.* **2013**, P07003 (2013).
- [28] M. Fagotti and F. H. L. Essler, “Stationary behaviour of observables after a quantum quench in the spin-1/2 Heisenberg XXZ chain,” *J. Stat. Mech.* **2013**, P07012 (2013).
- [29] B. Wouters, J. De Nardis, M. Brockmann, D. Fioretto, M. Rigol, and J.-S. Caux, “Quenching the anisotropic Heisenberg chain: Exact solution and generalized Gibbs ensemble predictions,” *Phys. Rev. Lett.* **113**, 117202 (2014).
- [30] B. Pozsgay, M. Mestyán, M. A. Werner, M. Kormos, G. Zaránd, and G. Takács, “Correlations after quantum quenches in the *XXZ* spin chain: Failure of the generalized gibbs ensemble,” *Phys. Rev. Lett.* **113**, 117203 (2014).
- [31] M. Fagotti, M. Collura, F. H. L. Essler, and P. Calabrese, “Relaxation after quantum quenches in the spin- $\frac{1}{2}$  Heisenberg XXZ chain,” *Phys. Rev. B* **89**, 125101 (2014).
- [32] J. De Nardis, B. Wouters, M. Brockmann, and J.-S. Caux, “Solution for an interaction quench in the Lieb-Liniger Bose gas,” *Phys. Rev. A* **89**, 033601 (2014).
- [33] G. Goldstein and N. Andrei, “Failure of the local generalized gibbs ensemble for integrable models with bound states,” *Phys. Rev. A* **90**, 043625 (2014).
- [34] M. Rigol, “Quantum quenches in the thermodynamic limit,” *Phys. Rev. Lett.* **112**, 170601 (2014).
- [35] F. H. L. Essler, G. Mussardo, and M. Panfil, “Generalized Gibbs ensembles for quantum field theories,” *Phys. Rev. A* **91**, 051602 (2015).

- [36] E. Iliovski, M. Medenjak, and T. Prosen, “Quasilocal conserved operators in the isotropic Heisenberg spin-1/2 chain,” *Phys. Rev. Lett.* **115**, 120601 (2015).
- [37] E. Iliovski, J. De Nardis, B. Wouters, J.-S. Caux, F. H. L. Essler, and T. Prosen, “Complete generalized Gibbs ensembles in an interacting theory,” *Phys. Rev. Lett.* **115**, 157201 (2015).
- [38] M. Moeckel and S. Kehrein, “Interaction quench in the Hubbard model,” *Phys. Rev. Lett.* **100**, 175702 (2008).
- [39] A. Rosch, D. Rasch, B. Binz, and M. Vojta, “Metastable superfluidity of repulsive Fermionic atoms in optical lattices,” *Phys. Rev. Lett.* **101**, 265301 (2008).
- [40] M. Moeckel and S. Kehrein, “Real-time evolution for weak interaction quenches in quantum systems,” *Ann. Phys.* **324**, 2146 – 2178 (2009).
- [41] M. Kollar, F. A. Wolf, and M. Eckstein, “Generalized Gibbs ensemble prediction of prethermalization plateaus and their relation to nonthermal steady states in integrable systems,” *Phys. Rev. B* **84**, 054304 (2011).
- [42] M. van den Worm, B. C. Sawyer, J. J. Bollinger, and M. Kastner, “Relaxation timescales and decay of correlations in a long-range interacting quantum simulator,” *New J. Phys.* **15**, 083007 (2013).
- [43] M. Marcuzzi, J. Marino, A. Gambassi, and A. Silva, “Prethermalization in a nonintegrable quantum spin chain after a quench,” *Phys. Rev. Lett.* **111**, 197203 (2013).
- [44] F. H. L. Essler, S. Kehrein, S. R. Manmana, and N. J. Robinson, “Quench dynamics in a model with tuneable integrability breaking,” *Phys. Rev. B* **89**, 165104 (2014).
- [45] G. P. Brandino, J.-S. Caux, and R. M. Konik, “Glimmers of a quantum KAM theorem: Insights from quantum quenches in one-dimensional Bose gases,” *Phys. Rev. X* **5**, 041043 (2015).
- [46] N. Nessi, A. Iucci, and M. A. Cazalilla, “Quantum quench and prethermalization dynamics in a two-dimensional Fermi gas with long-range interactions,” *Phys. Rev. Lett.* **113**, 210402 (2014).
- [47] B. Bertini and M. Fagotti, “Pre-relaxation in weakly interacting models,” *J. Stat. Mech.* **2015**, P07012 (2015).
- [48] B. Bertini, F. H. L. Essler, S. Groha, and N. J. Robinson, “Prethermalization and thermalization in models with weak integrability breaking,” *Phys. Rev. Lett.* **115**, 180601 (2015).
- [49] G. Menegoz and A. Silva, “Prethermalization of weakly interacting bosons after a sudden interaction quench,” *J. Stat. Mech.* **2015**, P05035 (2015).
- [50] M. Babadi, E. Demler, and M. Knap, “Far-from-equilibrium field theory of many-body quantum spin systems: Prethermalization and relaxation of spin spiral states in three dimensions,” *Phys. Rev. X* **5**, 041005 (2015).
- [51] C. N. Yang, “Some exact results for the many-body problem in one dimension with repulsive delta-function interaction,” *Phys. Rev. Lett.* **19**, 1312–1315 (1967).
- [52] M. Gaudin, “Un système à une dimension de fermions en interaction,” *Phys. Lett. A* **24**, 55 – 56 (1967).
- [53] B. Pozsgay, W.-V. van Gerven Oei, and M. Kormos, “On form factors in nested Bethe ansatz systems,” *J. Phys. A* **45**, 465007 (2012).
- [54] S. Belliard, S. Pakuliak, E. Ragoucy, and N. A. Slavnov, “The algebraic Bethe ansatz for scalar products in  $su(3)$ -invariant integrable models,” *J. Stat. Mech.* **2012**, P10017 (2012).
- [55] S. Belliard, S. Pakuliak, E. Ragoucy, and N. A. Slavnov, “Form factors in  $su(3)$ -invariant integrable models,” *J. Stat. Mech.* **2013**, P04033 (2013).
- [56] S. Pakuliak, E. Ragoucy, and N.A. Slavnov, “Form factors in quantum integrable models with  $r$ -invariant  $r$ -matrix,” *Nucl. Phys. B* **881**, 343 – 368 (2014).
- [57] S. Pakuliak, E. Ragoucy, and N.A. Slavnov, “Zero modes method and form factors in quantum integrable models,” *Nucl. Phys. B* **893**, 459 – 481 (2015).
- [58] S. Pakuliak, E. Ragoucy, and N. A. Slavnov, “Form factors of local operators in a one-dimensional two-component Bose gas,” *J. Phys. A* **48**, 435001 (2015).
- [59] M. Lewenstein, A. Sanpera, V. Ahufinger, B. Damski, A. Sen(De), and U. Sen, “Ultracold atomic gases in optical lattices: mimicking condensed matter physics and beyond,” *Adv. Phys.* **56**, 243–379 (2007).
- [60] M. A. Cazalilla, R. Citro, T. Giamarchi, E. Orignac, and M. Rigol, “One dimensional bosons: From condensed matter systems to ultracold gases,” *Rev. Mod. Phys.* **83**, 1405–1466 (2011).
- [61] D. M. Stamper-Kurn and M. Ueda, “Spinor Bose gases: Symmetries, magnetism, and quantum dynamics,” *Rev. Mod. Phys.* **85**, 1191–1244 (2013).
- [62] X.-W. Guan, M. T. Batchelor, and C. Lee, “Fermi gases in one dimension: From Bethe ansatz to experiments,” *Rev. Mod. Phys.* **85**, 1633–1691 (2013).
- [63] A. Schirotzek, C.-H. Wu, A. Sommer, and M. W. Zwierlein, “Observation of Fermi polarons in a tunable Fermi liquid of ultracold atoms,” *Phys. Rev. Lett.* **102**, 230402 (2009).
- [64] S. Nascimbène, N. Navon, K. J. Jiang, L. Tarruell, M. Teichmann, J. McKeever, F. Chevy, and C. Salomon, “Collective oscillations of an imbalanced Fermi gas: Axial compression modes and polaron effective mass,” *Phys. Rev. Lett.* **103**, 170402 (2009).
- [65] S. Palzer, C. Zipkes, C. Sias, and M. Köhl, “Quantum transport through a Tonks-Girardeau gas,” *Phys. Rev. Lett.* **103**, 150601 (2009).
- [66] C. Kohstall, M. Zaccanti, M. Jag, A. Trenkwalder, P. Massignan, G. M. Bruun, F. Schreck, and R. Grimm, “Metastability and coherence of repulsive polarons in a strongly interacting Fermi mixture,” *Nature* **485**, 615–618 (2012).
- [67] M. Koschorreck, D. Pertot, E. Vogt, B. Frohlich, M. Feld, and M. Kohl, “Attractive and repulsive Fermi polarons in two dimensions,” *Nature* **485**, 619–622 (2012).
- [68] J. Catani, G. Lamporesi, D. Naik, M. Gring, M. Inguscio, F. Minardi, A. Kantian, and T. Giamarchi, “Quantum dynamics of impurities in a one-dimensional Bose gas,” *Phys. Rev. A* **85**, 023623 (2012).
- [69] N. Spethmann, F. Kindermann, S. John, C. Weber, D. Meschede, and A. Widera, “Dynamics of single neutral impurity atoms immersed in an ultracold gas,” *Phys. Rev. Lett.* **109**, 235301 (2012).
- [70] R. Scelle, T. Rentrop, A. Trautmann, T. Schuster, and M. K. Oberthaler, “Motional coherence of Fermions immersed in a Bose gas,” *Phys. Rev. Lett.* **111**, 070401 (2013).
- [71] A. Klein, M. Bruderer, S. R. Clark, and D. Jaksch, “Dynamics, dephasing and clustering of impurity atoms in Bose-Einstein condensates,” *New J. Phys.* **9**, 411 (2007).
- [72] T. H. Johnson, S. R. Clark, M. Bruderer, and D. Jaksch, “Impurity transport through a strongly inter-

- acting bosonic quantum gas,” *Phys. Rev. A* **84**, 023617 (2011).
- [73] J. Goold, T. Fogarty, N. Lo Gullo, M. Paternostro, and Th. Busch, “Orthogonality catastrophe as a consequence of qubit embedding in an ultracold Fermi gas,” *Phys. Rev. A* **84**, 063632 (2011).
- [74] T. H. Johnson, M. Bruderer, Y. Cai, S. R. Clark, W. Bao, and D. Jaksch, “Breathing oscillations of a trapped impurity in a Bose gas,” *Europhys. Lett.* **98**, 26001 (2012).
- [75] C. J. M. Mathy, M. B. Zvonarev, and E. Demler, “Quantum flutter of supersonic particles in one-dimensional quantum liquids,” *Nature Phys.* **8**, 881–886 (2012).
- [76] F. Massel, A. Kantian, A. J. Daley, T. Giamarchi, and P. Törmä, “Dynamics of an impurity in a one-dimensional lattice,” *New J. Phys.* **15**, 045018 (2013).
- [77] A. Kantian, U. Schollwöck, and T. Giamarchi, “Competing regimes of motion of 1D mobile impurities,” *Phys. Rev. Lett.* **113**, 070601 (2014).
- [78] E. Burovski, V. Cheianov, O. Gamayun, and O. Lychkovskiy, “Momentum relaxation of a mobile impurity in a one-dimensional quantum gas,” *Phys. Rev. A* **89**, 041601 (2014).
- [79] O. Gamayun, O. Lychkovskiy, and V. Cheianov, “Kinetic theory for a mobile impurity in a degenerate Tonks-Girardeau gas,” *Phys. Rev. E* **90**, 032132 (2014).
- [80] O. Gamayun, “Quantum boltzmann equation for a mobile impurity in a degenerate Tonks-Girardeau gas,” *Phys. Rev. A* **89**, 063627 (2014).
- [81] O. Lychkovskiy, “Perpetual motion of a mobile impurity in a one-dimensional quantum gas,” *Phys. Rev. A* **89**, 033619 (2014).
- [82] P. Massignan, M. Zaccanti, and G. M. Bruun, “Polarons, dressed molecules and itinerant ferromagnetism in ultracold Fermi gases,” *Rep. Prog. Phys.* **77**, 034401 (2014).
- [83] M. Knap, C. J. M. Mathy, M. Ganahl, M. B. Zvonarev, and E. Demler, *Phys. Rev. Lett.* **112**, 015302 (2014).
- [84] A. G. Volosniev, H.-W. Hammer, and N. T. Zinner, “Real-time dynamics of an impurity in an ideal Bose gas in a trap,” *Phys. Rev. A* **92**, 023623 (2015).
- [85] N. J. Robinson, J.-S. Caux, and R. M. Konik, “Quantum stutter: arrested expansion without a lattice and impurity snaking,” ArXiv e-prints (2015), arXiv:1506.03502 [cond-mat.quant-gas].
- [86] J. Akram and A. Pelster, “Numerical study of localized impurity in a Bose-Einstein condensate,” ArXiv e-prints (2015), arXiv:1510.07138 [cond-mat.quant-gas].
- [87] C. Castelnuovo, J.-S. Caux, and S. H. Simon, “Driven impurity in an ultracold one-dimensional bose gas with intermediate interaction strength,” *Phys. Rev. A* **93**, 013613 (2016).
- [88] B. Sutherland, “Further results for the many-body problem in one dimension,” *Phys. Rev. Lett.* **20**, 98–100 (1968).
- [89] E. Lieb and D. Mattis, “Theory of ferromagnetism and the ordering of electronic energy levels,” *Phys. Rev.* **125**, 164–172 (1962).
- [90] P. Schlottmann, “Thermodynamics of the one-dimensional multicomponent Fermi gas with a delta-function interaction,” *J. Phys.: Condens. Matt.* **5**, 5869 (1993).
- [91] P. Schlottmann, “Ground-state and elemental excitations of the one-dimensional multicomponent Fermi gas with delta-function interaction,” *J. Phys.: Condens. Matt.* **6**, 1359 (1994).
- [92] O. I. Patu and A. Klumper, “Thermodynamics, contact and density profiles of the repulsive Gaudin-Yang model,” ArXiv e-prints (2015), arXiv:1512.07485 [cond-mat.quant-gas].
- [93] F. H. L. Essler, H. Frahm, F. Göhmann, A. Klümper, and V. E. Korepin, *The One-Dimensional Hubbard Model* (Cambridge University Press, 2005).
- [94] Y.-a. Liao, A. S. C. Rittner, T. Paprotta, W. Li, G. B. Partridge, R. G. Hulet, S. K. Baur, and E. J. Mueller, “Spin-imbalance in a one-dimensional Fermi gas,” *Nature* **467**, 567–569 (2010).
- [95] P. Fulde and R. A. Ferrell, “Superconductivity in a strong spin-exchange field,” *Phys. Rev.* **135**, A550–A563 (1964).
- [96] A. I. Larkin and Y. N. Ovchinnikov, “Inhomogeneous state of superconductors,” *Sov. Phys. JETP* **20**, 762–769 (1965).
- [97] K. Günter, T. Stöferle, H. Moritz, M. Köhl, and T. Esslinger, “*p*-wave interactions in low-dimensional Fermionic gases,” *Phys. Rev. Lett.* **95**, 230401 (2005).
- [98] H. Moritz, T. Stöferle, K. Günter, M. Köhl, and T. Esslinger, “Confinement induced molecules in a 1D Fermi gas,” *Phys. Rev. Lett.* **94**, 210401 (2005).
- [99] J. Heinze, J. S. Krauser, N. Fläschner, B. Hundt, S. Götzke, A. P. Itin, L. Mathey, K. Sengstock, and C. Becker, “Intrinsic photoconductivity of ultracold Fermions in optical lattices,” *Phys. Rev. Lett.* **110**, 085302 (2013).
- [100] A. Suto, “Percolation transition in the Bose gas,” *J. Phys. A* **26**, 4689 (1993).
- [101] E. Eisenberg and E. H. Lieb, “Polarization of interacting bosons with spin,” *Phys. Rev. Lett.* **89**, 220403 (2002).
- [102] B. I. Halperin and P. C. Hohenberg, “Hydrodynamic theory of spin waves,” *Phys. Rev.* **188**, 898–918 (1969).
- [103] B. I. Halperin, “Dynamic properties of the multicomponent Bose fluid,” *Phys. Rev. B* **11**, 178–190 (1975).
- [104] J. B. McGuire, “Interacting Fermions in one dimension. i. repulsive potential,” *J. Math. Phys.* **6**, 432–439 (1965).
- [105] J. N. Fuchs, D. M. Gangardt, T. Keilmann, and G. V. Shlyapnikov, “Spin waves in a one-dimensional spinor Bose gas,” *Phys. Rev. Lett.* **95**, 150402 (2005).
- [106] M. B. Zvonarev, V. V. Cheianov, and T. Giamarchi, “Spin dynamics in a one-dimensional ferromagnetic Bose gas,” *Phys. Rev. Lett.* **99**, 240404 (2007).
- [107] J. C. Zill, T. M. Wright, K. V. Kheruntsyan, T. Gasenzer, and M. J. Davis, “A coordinate Bethe ansatz approach to the calculation of equilibrium and nonequilibrium correlations of the one-dimensional Bose gas,” ArXiv e-prints (2016), arXiv:1601.00434 [cond-mat.quant-gas].
- [108] E. Kaminishi, R. Kanamoto, J. Sato, and T. Deguchi, “Exact yrast spectra of cold atoms on a ring,” *Phys. Rev. A* **83**, 031601 (2011).
- [109] J. Sato, R. Kanamoto, E. Kaminishi, and T. Deguchi, “Exact relaxation dynamics of a localized many-body state in the 1D Bose gas,” *Phys. Rev. Lett.* **108**, 110401 (2012).
- [110] J. Sato, R. Kanamoto, E. Kaminishi, and T. Deguchi, “Quantum dark solitons in the 1D Bose gas and the superfluid velocity,” ArXiv e-prints (2012),

- arXiv:1204.3960 [cond-mat.quant-gas].
- [111] E. Kaminishi, J. Sato, and T. Deguchi, “Recurrence time in the quantum dynamics of the 1D Bose gas,” ArXiv e-prints (2013), arXiv:1305.3412 [cond-mat.quant-gas].
- [112] E. Kaminishi, J. Sato, and T. Deguchi, “Exact quantum dynamics of yrast states in the finite 1D Bose gas,” ArXiv e-prints (2014), arXiv:1401.4262 [cond-mat.quant-gas].
- [113] E. Nicklas, M. Karl, M. Höfer, A. Johnson, W. Muesel, H. Strobel, J. Tomkovič, T. Gasenzer, and M. K. Oberthaler, “Observation of scaling in the dynamics of a strongly quenched quantum gas,” *Phys. Rev. Lett.* **115**, 245301 (2015).
- [114] We consider only systems with  $N$  even and  $M = 1$ . For fermions  $I_j \in \mathbb{Z} + \frac{1}{2}$ , and the ground state Fermi sea is unique:  $\{I\} = \{-\frac{(N-1)}{2}, -\frac{(N-1)}{2} + 1, \dots, \frac{(N-1)}{2}\}$ . For bosons  $I_j \in \mathbb{Z}$  and hence there are two configurations of the ‘Fermi sea’: we consider both  $\{I\} = \{-\frac{N}{2}, -\frac{N}{2} + 1, \dots, \frac{N}{2} - 1\}$  and  $\{I\} = \{-\frac{N}{2} + 1, -\frac{N}{2} + 2, \dots, \frac{N}{2}\}$  in the superposition of the initial state, Eq. (13).
- [115] K. Yang and Y.-Q. Li, “Rigorous proof of pseudospin ferromagnetism in two-component bosonic systems with component-independent interactions,” *Int. J. Mod. Phys. B* **17**, 1027–1033 (2003).
- [116] Y.-Q. Li, S.-J. Gu, Z.-J. Ying, and U. Eckern, “Exact results of the ground state and excitation properties of a two-component interacting Bose system,” *Europhys. Lett.* **61**, 368 (2003).
- [117] J.-S. Caux, A. Klauser, and J. van den Brink, “Polarization suppression and nonmonotonic local two-body correlations in the two-component Bose gas in one dimension,” *Phys. Rev. A* **80**, 061605 (2009).
- [118] A. Klauser and J.-S. Caux, “Equilibrium thermodynamic properties of interacting two-component bosons in one dimension,” *Phys. Rev. A* **84**, 033604 (2011).
- [119] O. I. Pâțu and A. Klümper, “Thermodynamics, density profiles, and correlation functions of the inhomogeneous one-dimensional spinor Bose gas,” *Phys. Rev. A* **92**, 043631 (2015).
- [120] We are currently limited to studying the single  $\sigma = \downarrow$  boson in the two-component Lieb-Liniger model, as the matrix elements of the majority component are not known to us, although there has been recent work in this direction [58].
- [121] M. T. Batchelor, M. Bortz, X. W. Guan, and N. Oelkers, “Collective dispersion relations for the one-dimensional interacting two-component Bose and Fermi gases,” *J. Stat. Mech.* **2006**, P03016 (2006).